https://doi.org/10.1016/j.jcsr.2021.106686

Structural behaviour of T-joints between high-strength S690 steel cold-formed circular hollow sections

Yi-Fei Hu[1,2], Kwok-Fai Chung[1,2*], Hao Jin[1,2], Huiyong Ban[3] and David A. Nethercot[4]

[1]*Department of Civil and Environmental Engineering,*
The Hong Kong Polytechnic University, Hong Kong SAR, China.
[2] *Chinese National Engineering Research Centre for Steel Construction (Hong Kong Branch)*
The Hong Kong Polytechnic University, Hong Kong SAR, China.
[3] *Department of Civil Engineering, Tsinghua University, China.*
[4] *Department of Civil and Environmental Engineering, Imperial College London, U.K.*
** Corresponding author: kwok-fai.chung@polyu.edu.hk*

ABSTRACT

This paper reports an experimental investigation into structural behaviour of T-joints between S690 cold-formed circular hollow sections (CFCHS). A total of twelve T-joints of both S355 and S690 CFCHS under *i) brace axial compression,* and *ii) brace in-plane moments* are tested to failure in order to examine their deformation characteristics, in particular, their joint resistances and failure modes. These tests are conducted with extensive instrumentation on both overall deformations of the T-joints and local deformations of their welded brace/chord junctions. Welding of all these T-joints between S690 CFCHS is carefully performed so that the heat input energy during welding varies narrowly between 1.2 and 1.5 kJ/mm. Standard tensile tests are also conducted on both flat and curved coupons extracted from the sections to provide mechanical properties for subsequent strength analysis.

All the tests have been successfully conducted. For those T-joints between S690 CFCHS under brace axial compression, chord plastification is always found to be a critical failure mode while for those T-joints between S690 CFCHS under brace in-plane moments, both brace fracture and chord punching shear failure are found to be critical at the end of the tests.

All the measured joint resistances of the T-joints between S690 CFCHS are found to be larger than those design resistances obtained with EN 1993-1-8 and Design Guide 1 of CIDECT. Consequently, this investigation provides structural insights and scientific data for possible improvements onto prediction capabilities of the design methods.

Keywords:

High strength steels; cold-formed circular hollow sections; CHS T-joints; overall plastic bending; local chord plastification.

NOTATIONS

C_f	Reduction factors to joint resistances for high strength steels
d_0	Outer diameter of the chord
d_1	Outer diameter of the brace
E	Young's modulus
f_y	Yield strength of steel
f_{y0}	Yield strength of the chord
f_u	Ultimate strength of steel
I	Welding current
k_p	Chord stress function defined by EN 1993-1-8

L	Span between two pinned supports of a T-joint between CFCHS
L_0	Length of the chord
L_1	Length of the brace
M_0	Bending moment applied to the chord
$M_{0,R}$	Plastic moment resistance of the chord
M_1	Bending moment applied to the brace
$M_{1,R}$	Plastic moment resistance of the brace
$M_{1,Rd}$	Design moment resistance of the brace to EN 1993-1-1
$M_{j,R}$	Measured moment resistance of the chord of a T-joint predicted to CIDECT or EN 1993-1-8 with a reduction factor for high strength steels
$M_{j,Rd}$	Design moment resistance of a T-joint
$M_{j,Rt}$	Measured moment resistance of a T-joint
$M_{0,R}$	Plastic moment resistance of the chord to EN 1993-1-1
$M_{pl,0}$	Plastic moment resistance of the chord
N_0	Axial force applied to the chord
$N_{pl,0}$	Axial resistance of the chord
N_x	Measured applied brace lateral force of the T-joint
$N_{x,R}$	Axial resistance predicted to CIDECT or EN 1993-1-8 with a reduction factor for high strength steels
$N_{x,Rt}$	Measured lateral resistance of the T-joint
N_z	Measured applied brace axial force of the T-joint
$N_{z,R}$	Axial resistance predicted to CIDECT or EN 1993-1-8 with a reduction factor for high strength steels
$N_{z,Rd}$	Design axial resistance of the T-joint
$N_{z,Rt}$	Measured axial resistance of the T-joint
$N_{z,Rt,N}$	Measured axial resistance of the T-joint according to a peak load
$N_{z,Rt,\delta}$	Measured axial resistance of the T-joint according to a 3% deformation limit
Q_u	Design strength function defined by CIDECT
Q_f	Chord stress function defined by CIDECT
V_0	Shear force in the chord
V_1	Shear force in the brace
n and n_p	Chord stress ratio
t_0	Wall thickness of the chord
t_1	Wall thickness of the brace
α	Chord length parameter
β	Brace to chord diameter ratio
2γ	Chord diameter to chord thickness ratio
γ_{M5}	Partial factor for resistance of joints in hollow section lattice girders accroding to EN 1993-1-8
τ	Ratio of brace wall thickness to chord wall thickness
Δ	Displacement measured with displacement transducers
$\Delta_{j,x}$	Lateral displacement of a T-joint
Δ_u	Displacement measured at failure
$\delta_{i,z}$	Chord indentation of the T-joint

$\delta_{j,z}$	Joint nodal displacement of the T-joint
ε_u	Elongation at tensile strength
ε_f	Elongation at fracture
θ_1	Angle between the chord and the brace of a T-joint
$\sigma_{p,Ed}$	Maximum compressive stress in the chord excluding the stress due to components parallel to the chord axis

1. Introduction

Since the 1970's, structural hollow sections (SHS) have been widely applied in construction projects around the world, including space frames in large enclosing structures, long span roofs of sports stadia and public terminals, and foot bridges, as shown in Figure 1. Circular hollow sections (CHS) are often preferred by architects because of their attractive appearance. Structural behaviour of both hot finished and cold-formed SHS of S235 to S460 steels has been studied by many researchers in the past forty years. Research outcomes of those studies have been widely published [1], and developed into various design specifications, such as Design Guide 1 of CIDECT [2], and EN 1993-1-8 [3], which are widely regarded as definitive technical guides for structural design for both hot finished and cold-formed SHS.

Owing to complex structural behaviour of different types of joints between CHS under various practical loading conditions, both experimental and numerical investigations on these joints have been conducted in the past decades. Research findings of these investigations have facilitated development of various design methods for engineering applications through international collaboration among researchers and engineers. It should be noted that design recommendations for these joints were published by the International Institute of Welding (IIW) Sub-commission XV-E in 1981, and then, in 1991[4]. More recently, EN 1993-1-8 [3] adopted the design recommendations presented in the 2nd edition of IIW recommendations [5], and the latest version of Design Guide 1 of CIDECT [2] follows closely to the 3rd edition of IIW recommendations [6].

Owing to technological advancement in steel-making in the past twenty years, high strength steels with yield strengths equal to or exceeding 460 N/mm^2, such as S460, S550 and S690 steels, are produced in many parts of the world. Their typical applications are large lifting equipment in which strong but light structures, all with large strength to self-weight ratios, are highly beneficial to their daily operation. In general, S690 cold-formed circular hollow sections (CFCHS) are highly efficient structural members for construction, and they are readily manufactured through transverse bending and longitudinal welding of steel plates to suit specific requirements on cross-sectional dimensions and quantities. Hence, it is highly desirable to develop complementary design rules to assess the structural behaviour of these S690 CFCHS and their joints under various actions.

It should be noted that as many of these high strength S690 steel plates achieve their strengths through heat-treatment, such as quenching (Q) and tempering (T) during their production, i.e. S690-QT, so that both the processes of heating up and cooling down are carefully controlled during steel-making to ensure that grain sizes of their microstructures are sufficiently small in order to attain favourable mechanical properties. However, welding of these S690-QT steel plates may cause phase transformation, re-crystallization and grain growth on their microstructures if the heat energy input of the welding is not controlled properly. It is well established in the fields of materials science and metallurgy that reduction in the mechanical properties in the heat-affected-zones of these S690-QT welded sections are often directly related to their cooling rates, $t_{8/5}$, which is the time elapsed for their temperature to drop from

800 ^{o}C to 500 ^{o}C. In general, the cooling rate $t_{8/5}$ is heavily dependent on various welding procedures and parameters, such as the heat input energy during welding, the plate thickness, and the pre-heating temperatures.

1.1 Research work on joints between high strength CHS

Figure 2 illustrates typical configuration of the T-joints between CFCHS. Up till the presence, experimental investigations on the T-joints between S690 CFCHS are found to be limited in both numbers and section sizes in general. It is straightforward to test simply supported T-joints under brace axial compression, and typical failure modes due to i) local chord plastification, and ii) overall plastic bending are commonly found. However, these two modes may not be easily identified separately, and their corresponding section resistances are rather difficult to be assessed individually owing to interaction between the applied forces and the induced bending moments, both acting onto the chords. For those T-joints under brace in-plane moments, the critical failure mode is typically a section failure of the braces under in-plane moments while local plastification in the welded brace/chord junctions may become apparent.

A total of four T-joints between hot-finished CHS under brace axial compression were tested and reported by Choi et al. [7], and the measured yield strength of these CHS was 517 N/mm^2. All these four T-joints failed in local chord plastification. Kim et al. [8] reported an experimental study on a total of twelve T-joints between high strength CHS under cyclic in-plane moments; the measured yield strengths of these CHS were 464 and 584 N/mm^2. From these tests, the T-joints were found to possess large joint resistances against local chord plastification without any significant reduction in ductility, when compared with those of joints between S355 CHS.

It should be noted that existing design methods given for joints between high strength CHS in the Design Guide 1 of CIDECT and EN 1993-1-8 were mostly developed according to extensive numerical results as well as re-assessments of test results in the literature [9]. Since there were insufficient test data on joints between high strength CHS available at that time, both strength reduction factors and limitations on the tensile-to-yield strength ratios, f_u / f_y , were introduced to provide simple and safe structural design on the expense of certain structural efficiency. In recent years, a number of experimental investigations on joints between high strength CHS and RHS have been reported in the literature, and various types of X- and K-joints with different cross-section geometry were tested to provide valuable test data for re-evaluating the current design methods [9, 10, 11, 12, 13, 14, 15, 16]. It should be noted that analyses on experimental results on X-joints between high strength CHS and RHS subjected to brace axial compression suggested that the reduction factors given in EN 1993-1-8 might be too conservative for S690 steels [17, 18].

In general, additional experimental and numerical investigations on the structural behaviour of typical joints between high strength S690 CFCHS are always desirable to demonstrate applicability of existing design methods and suitability of various reduction factors in achieving a balance between structural adequacy and efficiency at the same time.

1.2 Related research on structural behaviour of high strength S690 steels by the authors

In order to promote effective use of high strength S690 steels in construction, a comprehensive research and development programme is undertaken by the authors to investigate mechanical properties of S690 steels as well as structural behaviour of S690 steel sections. One of the key research areas is to investigate effects of manufacturing processes onto structural behaviour of S690 steel members and joints, and these include:

a) microstructural changes in heat-affected zones of welded sections and joints [19];
b) reductions in mechanical properties of welded sections with various heat input energy during welding [20];
c) thermo-mechanical analyses on residual stresses of cold-formed structural hollow sections due to i) transverse bending, and ii) longitudinal welding [21, 22]; and
d) early yielding in both cold-formed and welded sections due to presence of residual stresses, and hence, reductions in member resistances and joint resistances [23, 24].

In general, reductions in the mechanical properties, in particular, both the yield and the tensile strengths, of these S690-QT welded sections are demonstrated to be significantly smaller than those reported in the literature, especially in those steel plates with thicknesses in the range of 6 to 16 mm. The corresponding cooling rates $t_{8/5}$ for welding of 16 mm thick steel plates with various heat input energy, q , at 1.0, 1.5 and 2.0 kJ/mm are 5.5, 12.4 and 22.0 seconds respectively. According to various research mentioned above, it is demonstrated that:

- For S690 welded sections under compression, a total of twelve S690 welded H-sections of 4 different cross-sectional dimensions with butt-welded joints at their mid-heights were tested. The nominal thicknesses of these steel plates were 6, 10 and 16 mm. It was demonstrated that there was no reduction in the compression resistances of these sections at all when their heat input energy during welding was kept to or below 2.0 kJ/mm.

- For S690 welded sections under tension, a total of eighteen cylindrical coupons of S690 welded sections with butt-welded joints at their mid-lengths were tested. The nominal thickness of the steel plates is 16 mm, and the diameters along gauge lengths the cylindrical coupons are 5.0 mm. While it was demonstrated that there was only a small degree of softening in these coupons of the welded sections, and hence, a small reduction in their yield strengths, there was no reduction in their tensile strengths when the heat input energy during welding was kept to or below 1.0 kJ/mm. However, for welded sections with a heat input energy equal to 5.0 kJ/mm, both the yield and the tensile strengths are reduced according to the reduction factors at 0.70 and 0.83 respectively [20]. There are also significant reductions in both strain hardening and elongation limit at fracture.

Consequently, it is highly desirable to extend the experimental investigation to examine the structural behaviour of the high strength S690 welded sections with a good control on the heat input energy, q, during welding, and to assess the deformation characteristics of typical joints under i) axial compression, and ii) in-plane moments.

1.3 Objectives and scope of work

This paper reports an experimental investigation into the structural behaviour of a total of four T-joints between S355 CFCHS, and eight T-joints between S690 CFCHS. All of these T-joints were fabricated with a proper control on the heat input energy during welding, and they were tested to structural failure to examine their deformation characteristics, in particular, joint resistances, ductility and critical modes of failure. There are a total of four series of tests in the test programme, and they are classified according to different types of actions and different dimensions of the braces as follows:

- Structural tests on T-joints under brace axial compression
  - Series P1 - 150/250: Joints T1, T2 and T3;
  - Series P2 - 200/250: Joints T4, T5 and T6.
- Structural tests on T-joints under brace in-plane moments
  - Series Q1 - 150/250: Joints T7, T8 and T9;
  - Series Q2 - 200/250: Joints T10, T11 and T12.

Figure 3 shows the cross-sectional dimensions of the four CFCHS. The test programme for T-joints of the present investigation is summarized in Table 1 together with geometrical dimensions and key parameters of the CFCHS.

It should be noted that these joint tests are conducted with extensive instrumentation on both overall deformations of the T-joints and local deformations of their welded brace/chord junctions. Moreover, a non-contact measurement technique with high precision, namely, a Digital Image Correlation (DIC) technique [25, 26], is employed to measure surface deformations of the welded brace/chord junctions of selected tests. Comprehensive data analysis and interpretation on these measured data is also performed.

As the existing design methods for the T-joints between CHS are primarily developed according to those test results of T-joints between S355 CHS together with supplementary numerical results of finite element modelling [9, 10], there is a clear need to verify validity of these design methods when they are extended to cover T-joints between S690 CFCHS. Hence, the measured resistances of these T-joints are compared against the design resistances obtained with those relevant design rules in both EN 1993-1 and Design Guide 1 of CIDECT, and structural adequacy and efficiency of the design methods on these T-joints is assessed.

The key areas of interest of the present investigation include:

a) deformation characteristics with different degrees of mobilization in strength and ductility, and failure modes of these T-joints between S690 CFCHS, when compared with those of T-joints between S355 CFCHS;
b) applicability of existing design methods to predict resistances of these T-joints between S690 CFCHS with a proper control of the welding process.

1.4 Fabrication of CFCHS

The cold-formed circular hollow sections (CFCHS) were fabricated in a qualified steelwork fabricator from steel plates through a series of processes as follows:

i) press-braking of plate edges with a circular punch,
ii) transverse bending of plates using a three-roller bending machine, and
iii) longitudinal welding using a gas metal arc welding (GMAW) method.

The fabrication processes of the CFCHS are illustrated in Figure 4. After fabrication of the CFCHS for the braces and the chords, edge preparation was performed at the brace ends in order to make profiled connecting surfaces for joint welding.

Table 2 summarizes the measured geometric dimensions of both the chords and the braces of all the joints. It should be noted that all the brace/chord junctions between these CFCHS were welded with a combination of i) fillet welds, and ii) full penetration butt welds by a highly skilled welder who was able to perform the welding consistently. It should be noted that:

- the welding electrode E71T-1 with a diameter of 1.2 mm according to AWS A5.20 [27] is adopted for welding of S355 steels; and
- for welding of S690 steels, the welding electrode ER110S-G with a diameter of 1.2 mm according to AWS A5.28 [28] is adopted.

Both chemical compositions and mechanical properties of these welding electrodes are summarized in Tables 3 and 4.

Welding details at both the crown points and the saddle points of the junctions are illustrated in Figure 5 while typical measured weld sizes at both the crown and the saddle points of each of the welded brace/chord junctions of the T-joints are shown in Table 5. It should be noted that the heat input energy during welding of all the S690 CFCHS and their welded brace/chord junctions were found to range from 1.2 to 1.5 kJ/mm. Based on the experiences on similar investigations [20, 29], there was no significant reduction in the mechanical properties of these S690 welded sections under this level of heat input energy.

It should be noted that residual stresses due to i) transverse bending, and ii) longitudinal welding in these S690 CFCHS were investigated extensively through a complementary experimental and numerical investigation [21, 22]. While the longitudinal residual stresses due to transverse bending were found to be fairly uniformly distributed throughout the circumferences of these CFCHS, highly localized longitudinal residual stresses due to longitudinal welding were found to be present in the vicinity of the welding seams. As these residual stresses were self-equilibrant, they were commonly considered to have little effects on the section resistances of these CFCHS though they caused pre-mature yielding in some parts of these sections [18, 22, 30].

1.5 Material properties

Standard tensile tests were carried out according to BS EN ISO-6892-1 [31] on curved coupons extracted from both the S355 and the S690 CFCHS to obtain mechanical properties for subsequent strength analysis. Typical locations of these curved coupons cut from the CFCHS, and their shapes and dimensions are illustrated in Figure 6. The test set-up is shown in Figure 7a), and strain gauges are attached to both sides of the curved coupons, as shown in Figure 7b), to measure their elongations throughout the tests. Owing to the page limit, only the measured stress-strain curves of the curved coupons extracted from various S690 CFCHS of different dimensions are plotted in Figure 7c) for easy comparison. Key results of these tensile tests, and hence, the mechanical properties of all the S355 and the S690 CFCHS are presented in Table 6.

2. Experimental Investigation

A total of twelve T-joints between CFCHS are tested in the present investigation, and both S355 and S690 CFCHS are covered in order to examine the structural behaviour of these T-joints with different steel grades as well as different dimensions of the braces under i) brace axial compression, and ii) brace in-plane moments.

2.1 Test programme

Details of various test series are described as follows:

- Series P1 - 150/250: Joints T1, T2 and T3 under brace axial compression
  In Joint T1, there is a brace of S355 CFCHS 150×6 mm welded onto a chord of S355 CFCHS 250×10 mm. In Joint T2, the dimensions of both the brace and the chord are the same as those in Joint T1, but with S690 steels. Joint T3 is nominally identical to Joint T2, and it serves as a repeat test for confirmation of the structural behaviour. Hence, this series is devised to compare the structural behaviour of the T-joints with chords of S355 CFCHS and of S690 CFCHS under axial compression applied through the braces with a relatively small diameter, i.e. d_1 = 150 mm.

- Series P2 - 200/250: Joints T4, T5 and T6 under brace axial compression
  In Joint T4, there is a brace of S355 CFCHS 200×6 mm welded onto a chord of S355 CFCHS 250×10 mm. In Joint T5, the dimensions of both the brace and the chord are the same as those in Joint T4, but with S690 steels. Joint T6 is nominally identical to Joint T5 except the thickness of the brace is increased from 6 to 10 mm, and it serves as a variant to Joint T5. Hence, this series is devised to compare the structural behaviour of the T-joints with chords of S355 CFCHS and of S690 CFCHS under axial compression applied through the braces with a relatively large diameter, i.e. d_1 = 200 mm.

  It should be noted that the effects of cross-sectional dimensions of the braces, d_1 and t_1, onto the axial resistances of the T-joints are also examined. As the diameters of the braces are increased to 200 mm, the axial resistances of all the T-joints in Series P2 are expected to be larger than those of the T-joints in Series P1. All the dimensions and their geometrical ratios of these T-joints are considered to be typical in practice, and chord plastification is expected to be critical in all these joints.

- Series Q1 - 150/250: Joints T7, T8 and T9 under brace in-plane moments

  All the T-joints in this series are similar to those in Series P1 in terms of both the steel grades and the dimensions of the braces, i.e. Joints 1 and 7 are the same while Joints 2 and 3, and Joints 8 and 9 are the same. The only difference is the presence of the brace in-plane moments in this series, instead of the brace axial compression in Series P1.

- Series Q2 - 200/250: Joints T10, T11 and T12

  Similarly, all the T-joints in this series are similar to those in Series P2 in terms of both the steel grades and the dimensions of the braces, i.e. Joints 4 and 10 are the same while Joints 5 and 6, and Joints 11 and 12 are the same. The only difference is the presence of the brace in-plane moments in this series, instead of the brace axial compression in Series P2. All the dimensions and their geometrical ratios of these T-joints are considered to be typical in practice. Among the four common modes of failure in T-joints between CHS under in-plane bending, namely, i) chord plastification, ii) chord punching shear failure, iii) brace failure, and iv) weld fracture, both brace failure and chord punching shear failure are expected to be critical in these joints while local deformations in the brace/chord junctions may be apparent. It should be noted that weld fracture is readily prevented through the use of a proper welding procedure performed by an experienced welder.

Refer to Table 1 for the cross-sectional dimensions of both the chords and the braces together with their section classifications according to EN 1993-1-1 [32]. It should be noted that:

i) the ratio of brace to chord diameter, $\beta = d_1 / d_0$, is assigned to range from 0.6 to 0.8, and
ii) the ratio of brace wall thickness to chord wall thickness, $\tau = t_1 / t_0$, is assigned to range from 0.8 to 1.0.

While the distance between the two simple supports of the T-joints are 1500 mm, the lengths of the chord, L_0, and of the brace L_1 are 1200 and 600 mm, respectively, as shown in Figure 2.

3 Structural tests on T-joints under brace axial compression – Series P1 and P2

The experimental investigation into the structural behaviour of the T-joints under brace axial compression are described in this section. Details of test set-up, instrumentation and loading procedures, deformation characteristics and failure modes of these joints are thoroughly presented as follows.

3.1 Test set-up, instrumentation and loading procedures

All the joint tests under brace axial compression were carried out with a Servo Hydraulic Control Testing System with a loading capacity of 1,000 tons, as shown in Figure 8a), and typical test set-up and instrumentation is illustrated in Figure 8b).

In each test, the chord of the T-joint was simply supported at both ends through steel pins, i.e. while in-plane rotations were allowed at both ends, lateral movement along long slotted holes in the base plate of the support was allowed at one end only. Two laser levels were placed in front of and to the left of the T-joint to ensure good alignment between the centreline of the brace and the centreline of the loading attachment. A total of twelve displacement transducers, namely, Transducers L01 to L12, were used to measure both horizontal and vertical displacements of specified locations of the T-joints, and deformations at both the crown and the saddle points of the welded brace/chord junctions were measured systematically. Moreover, four strain gauges, namely, SG1 to SG4, each with a gauge length of 5 mm, were mounted onto the brace to monitor its axial strains throughout the test. A non-contact measurement method, namely, Digital Imaging Correlation technique, is also adopted to measure surface deformation fields of the brace/chord junctions of selected T-joints. Refer to Section 5 for further details.

In each test, an axial compression force was applied onto the top of the brace of the T-joint, and the following loading procedure was adopted:

a) Before testing, a preloading process was conducted. A force at 30% of the predicted joint resistance of the T-joint was applied. Then, the force was reduced at a rate of 150 kN per minute. This process was repeated for a total of three times to minimize initial bedding.
b) In the initial stage of testing, the force was applied at a rate of 50 kN per minute, and it was steadily increased up to 80% of the predicted joint resistance.
c) Then, the force was applied through displacement control, and an axial displacement was applied at a rate of 0.3 mm/min until apparent unloading; the peak load $N_{z,Rt,N}$ was recorded.
d) Finally, the axial displacement was applied at a rate of 0.5 mm/min, and the test was terminated when the value of the force was found to drop below 80% of the peak load.

The applied force, N_z , was measured together with all the readings of the transducers and the strain gauges at small time intervals, and all these data were recorded in the data logger for subsequent analysis.

It should be noted that the initial out-of-straightness of the T-joints were measured before testing, as shown in Figure 8c). As these T-joints were fabricated in a qualified steelwork fabricator, the workmanship of fabrication, in particular, pre-welding alignment and distortion control, was guaranteed. In each test, measurements were made to each T-joint after it was installed onto the supports, and adjusted carefully for proper alignment. As both the values of v1 and v2 were found to be smaller than 0.5 to 1.0 mm, the initial out-of-straightness of the T-joints were considered to be very small.

3.2 Test results

All these tests have been completed successfully, and the test results are presented in the following sections while key data are summarized in Table 7.

3.2.1 Failure modes

Figure 9 illustrates the deformed shapes of all the six T-joints at large deformation stages of the tests, and local chord plastification in all the chords of the T-joints are apparent. Section distortion in the form of local indentation of the welded brace/chord junction due to extensive plastic deformations is also evident, as shown in Figure 10.

As the chords of all the T-joints are subjected to both shear forces and bending moments as well as co-existing axial compression forces through the braces, as shown in Figure 11, there is a significant reduction to the section resistances of the chords at the welded junctions after extensive plastic deformations under high brace axial compression.

After termination of the tests, all the T-joints were inspected closely, and no crack in the welded junctions nor any fracture in the welds was found. Typical detail of the welded connections at the crown points of the T-joints after etching is shown in Figure 10d). Hence, there is no evidence to show any significant deterioration in the structural behaviour of the T-joints between S690 CFCHS due to welding in the presence of brace axial forces.

3.2.2 Applied force-nodal displacement curves

In each of the six T-joints, the vertical nodal displacement of the joint, $\delta_{j,z}$, is given by:

$$\delta_{j,z} = \frac{\Delta_6 + \Delta_7}{2} \tag{1}$$

where

Δ_6 and Δ_7 are the vertical displacements measured by Transducers L06 and L07 shown in Figure 8b).

The applied force versus nodal displacement (N_z - $\delta_{j,z}$) curves of the T-joints are shown in Figure 12. It should be noted that:

- In Series P1-150/250, the curve of Joint T1 exhibits a load-deformation characteristic with *limited ductility* while the curves of both Joints T2 and T3 show a significant reduction in resistances after unloading, i.e. a non-ductile characteristic.
- In Series P2-200/250, a fairly ductile load-deformation characteristic is evident in the curve of Joint T4. However, the curves of both Joints T5 and T6 are considered to be very different as they exhibit a non-ductile characteristic after the peak loads are attained.

3.2.3 Applied force-chord indentation curves

In each of the six tests, the maximum indentation, or distortion, of the T-joint is found to occur at the crown point of the chord. Hence, this deformation, namely, chord indentation $\delta_{i,z}$ of the T-joint, is taken as the relative vertical deformation at the crown points to the centreline of the chord, which is given by:

$$\delta_{i,z} = \frac{\Delta_4 + \Delta_5}{2} - \delta_{j,z} \tag{2}$$

where

Δ_4 and Δ_5 are the vertical displacements measured by Transducers L04 and L05 shown in Figure 8b).

$\delta_{j,z}$ is the vertical nodal displacement of the joint given by Eqn. (1).

The applied force versus chord indentation (N_z - $\delta_{i,z}$) curves of the T-joints are also shown in Figure 12. It should be noted that:

- In Series P1-150/250, the curves exhibit a deformation characteristic with limited ductility, and there are significant reductions in the joint resistances after gross local indentations in the chords have taken place.
- Similarly, in Series P2-200/250, these curves exhibit a non-ductile characteristic, and the presence of gross local indentations in the chords causes significant reductions to the joint resistances.
- In both Series P1 and P2, the maximum chord indentations of all the T-joins between S690 CFCHS are found to exceed the deformation (indentation) limits at 3% of the chord diameters, i.e. 7.5 mm.

In general, the applied force versus chord indentation (N_z - $\delta_{i,z}$) curves are considered to be representative to the overall structural behaviour of these T-joints under brace axial compression.

3.2.4 Measured strains

Figure 13 plots the measured strains of the braces of all the T-joints. It is shown that all the braces remain elastic throughout the entire deformation ranges as these strains are well below the yield strains of the S355 and the S690 steels, i.e. 0.169 % and 0.329% respectively.

3.2.5 Joint resistances

The measured brace axial resistance, $N_{z,Rt}$, of each T-joint is defined as follows:

i) the peak load, $N_{z,Rt,N}$, if it occurs prior to the deformation limit, which is obtained directly in the test, or

ii) the applied force corresponding to a deformation limit, $N_{z,Rt,\delta}$, i.e. a limit to local chord indentation at 3% of the outer diameter of the chord, or 0.03 d_0 , according to Design Guide 1 of CIDECT [2, 33].

It is observed from the applied force versus chord indentation (N_z - $\delta_{i,\delta}$) curves of all the tests that the applied forces reach their peak values prior to any deformation limit, i.e. 0.03 d_0 or 7.5 mm, is reached. Hence, these peak values of the applied forces are taken as their joint resistances against brace axial compression, and these joint resistances, $N_{z,Rt}$, are summarized in Table 7. It is shown that

i) The measured yield strength of the 10 mm S690 steel plate is 766 N/mm^2 while that of the 10 mm S355 steel plate is 365 N/mm^2, as shown in Table 6. Hence, the ratio between these two values is 2.10.

ii) However, the measured resistances of Joints T2 and T3 with S690 steels are 1.58 and 1.69 times of that of Joint T1 with S355 steels respectively. Similarly, the measured resistances of Joints T5 and T6 with S690 steels are 1.80 and 1.73 times of that of Joint T4 with S355 steels respectively.

iii) Hence, structural benefits owing to an increase in yield strengths cannot be fully achieved in those T-joints with S690 steels, when compared with those with S355 steels, because of a reduced strain hardening. Hence, a reduction factor should be applied in design to allow for different extents of strain hardening after yielding when S690 steels are used. Refer to Section 6 for further details.

4. Structural tests on T-joints under brace in-plane moments – Series Q1 and Q2

The experimental investigation into the structural behaviour of the T-joints under brace in-plane moments are described in this section. Details of test set-up, instrumentation and loading procedures, deformation characteristics and failure modes of these joints are thoroughly presented as follows.

4.1 Test set-up and loading procedures

All the joint tests under brace in-plane moments were carried out with a 150 tons loading system with a hydraulic jack, as shown in Figure 14a), and typical test set-up and instrumentation is illustrated in Figure 14b). In each test, the chord of the T-joint was simply supported at both ends through steel pins, i.e. while in-plane rotations were allowed at both ends, lateral movement along long slotted holes in the base plate of the support was allowed at one end only. Both the vertical plane of the T-joint and the line of action of the hydraulic jack were carefully aligned with the help of two laser levels. A total of eight displacement transducers, namely, Transducers L01 to L08, were used to measure both horizontal and vertical displacements of specified locations of the T-joints, and deformations at both the crown and the saddle points of the welded brace/chord junctions were measured systematically. Moreover, three strain gauges, namely, SG1 to SG3, each with a gauge length of 5 mm, were mounted onto the brace to monitor its axial strains throughout the test. The Digital Imaging Correlation technique is also adopted to measure surface deformation fields of the brace/chord junctions of selected T-joints. Refer to Section 5 for further details.

In each test, a lateral force was applied onto the top of the brace of the T-joint, and the following loading procedure was adopted:

a) Before testing, a preloading process was conducted. A force at 30% of the predicted joint resistance of the T-joint was applied. Then, the force was reduced at a rate of about 20 kN per minute. This process was repeated for a total of three times to minimize initial bending.

b) In the initial stage of testing, the force was applied at a rate of about 20 kN per minute, and it was steadily increased up to 80% of the predicted joint resistance. Then, the force was applied at a reduced rate of about 5 to 10 kN per minute or a displacement of about 1 to 2 mm per minute up to unloading; the peak load $N_{x,Rt,N}$ was recorded.

c) The test was terminated when the value of the force was found to drop below 80% of the peak load.

The applied force, N_x , was measured together with all the readings of the transducers and the strain gauges at small time intervals, and all these data were recorded in the data logger for subsequent analysis.

It should be noted that the initial out-of-straightness of the T-joints were measured before testing, as shown in Figure 14c). As these T-joints were fabricated in a qualified steelwork fabricator, the workmanship of fabrication, in particular, pre-welding alignment and distortion control, was guaranteed. In each test, measurements were made to each T-joint after it was installed onto the supports, and adjusted carefully for proper alignment. As both the values of v1 and v2 were found to be smaller than 0.5 to 1.0 mm, the initial out-of-straightness of the T-joints were considered to be very small.

4.2 Test results

All these tests have been completed successfully, and the test results are presented in the following sections while key data are summarized in Table 8.

4.2.1 Failure modes

Figure 15 illustrates the deformed shapes of all the six T-joints at large deformation stages of the tests, and gross bending deformations in both the braces and the chords in all the T-joints are also apparent. In general, no weld fracture was found in any of these joints in close inspection after termination of the tests. As the welded brace/chord junctions of these joints are subjected to co-existing bending moments and shear forces, as shown in Figure 16, significant local deformations in the brace/chord junctions are evident. After a careful examination into the structural behaviour of these T-joints, the deformed shapes of the junctions of all these T-joints after testing are shown in Figures 17 and 18 as follows:

- Brace failure with local buckling under bending in both T-joints between S355 CFCHS, i.e. Joints T7 and T10, is apparent.

- For those T-joints between S690 CFCHS, brace failure with fracture in the heat-affected zones at the brace bases in Joints T8 and T9 as well as Joint T11 are apparent while chord punching shear failure in Joint T12 is critical.

- Typical detail of a fractured heat-affected zone of the welded brace/chord junction is shown in Figure 18c).

It should be noted that gross plastic deformations in the chords are also apparent.

4.2.2 Applied force-nodal displacement curves

In each of the six T-joints, the lateral displacement of the loaded point of the brace, $\Delta_{j,x}$, is given by:

$$\Delta_{j,x} = \Delta_1 - \frac{\Delta_4 - \Delta_6}{2} \tag{3}$$

where

Δ_1 , Δ_4 and Δ_6 are the lateral displacements measured by Transducers L01, L04 and L06 shown in Figure 14b).

The applied force versus nodal displacement (N_x - $\Delta_{j,x}$) curves of the T-joints are shown in Figures 17b) and 18b). It should be noted that $\Delta_{j,x}$ includes inelastic deformations from both chord indentation and brace yielding in the present study.

- In Series Q1-150/250, the curve of Joint T7 exhibits a highly ductile load-deformation characteristic as its lateral displacement $\Delta_{j,x}$ exceeds 135.0 mm. The curves of both Joints T8 and T9 show a significant increase in strength together with a reduced ductility, when compared with that of Joint T7. After full mobilization of the design joint resistances, a sudden fracture in the heat-affected-zones of the braces occurs after the lateral displacements $\Delta_{j,x}$ of Joints T8 and T9 reach 84.7 and 87.7 mm respectively.

- In Series Q2-200/250, a highly ductile load-deformation characteristic is also evident in the curve of Joint T10 as its lateral displacement $\Delta_{j,x}$ exceeds 104.6 mm. The curves of both Joints T11 and T12 are considered to have a significant increase in strength together with a reduced ductility, when compared with that of Joint T10. After full mobilization of the joint resistance in Joint T11, a sudden fracture in the heat-affected-zones of the brace base occurs after its lateral displacement $\Delta_{j,x}$ reaches 67.7 mm. For Joint T12, a sudden punching shear failure occurs in the chord after its lateral displacement $\Delta_{j,x}$ reaches 88.4 mm.

It should be noted that as brace failure is observed among Series Q1 and Q2, the 3% deformation limit is not considered in determining the resistances of these T-joints.

4.2.3 Measured strains

Figure 19 plots the measured strains of the braces of all the T-joints. It is shown that all the measured strains are shown to be smaller than the yield strains of the S355 and the S690 steels, i.e. 0.169 % and 0.329% respectively. Unfortunately, as these strains are installed at the mid-height of the braces, these data do not reflect the critical yielding conditions of the braces at their bases.

4.2.4 Joint resistances

The measured in-plane moment resistance, $M_{j,Rt}$, of each T-joint is defined as the moment corresponding to the lateral load resistance, $N_{x,Rt}$, obtained directly in the test, and these joint resistances are summarized in Table 8. It is shown that

i) The measured yield strength of the 10 mm S690 steel plate is 766 N/mm^2 while that of the 10 mm S355 steel plate is 365 N/mm^2, as shown in Table 6. Hence, the ratio between these two values is 2.10.
ii) However, the measured resistances of Joints T8 and T9 with S690 steels are 1.82 and 1.85 times of that of Joint T7 with S355 steels respectively. Similarly, the measured resistances of Joints T11 and T12 with S690 steels are 1.73 and 1.76 times of that of Joint T10 with S355 steels respectively.

iii) Hence, structural benefits owing to an increase in yield strengths cannot be fully achieved in those T-joints with S690 steels, when compared with those with S355 steels. That is similar to those test results of Series P1 and P2.

As the moment resistances of those T-joints between S690 CFCHS have been readily mobilized well before brace failure with HAZ fracture, the sudden fracture does not cause a significant reduction in strength though there is definitely a reduction in ductility.

5 Assessment on deformation fields at the welded junctions

It was important to investigate the deformations of the welded brace/chord junctions of the T-joints under the presence of the applied forces. Thus, a DIC system with two high resolution cameras was employed to monitor the surface deformations of the welded junctions throughout the tests. The set-up of the DIC system is shown in Figure 20a) while Figure 20b) illustrates typical images captured from the cameras. According to the focal lengths of the two digital cameras, an area of 240 mm × 200 mm was adopted to cover the welded junctions of the T-joints, and their deformation fields were obtained through continuous tracking of speckle patterns on the junction surfaces. Surface principal strain contours in the vicinity of the welded junctions were readily evaluated using correlation algorithms. It should be noted that in each test, an image was taken by each of the cameras before testing as a reference. Then, images were captured at an interval of 60 seconds throughout the test. Details of the measured deformation fields of both Joints T3 and T11 are described as follows.

5.1 Deformation fields of Joint T3 under brace axial force

Figure 21a) presents the surface principal compressive strain contours of Joint T3 at five different deformation stages, namely, Stages D1 to D5, together with the corresponding force-displacement curves at various reference points of the welded junctions, i.e. Points R1 to R7. It is evident that:

a) Surface principal strains of the junction are found to be generally small when the applied axial force N_z is equal to 396 kN or 0.4 $N_{z,Rt}$, i.e. Stage D1. The maximum surface principal strain is found to occur at Point R4, i.e. the saddle point of the junction, at a value of 0.48%. Thus, Point R4 may be considered to be a stiff point in the junction which is always ready to take up a high proportion of the axial force, and hence, first yielding in the chord will take place at Point R4.

b) When the applied force N_z reaches 737 kN or 0.8 $N_{z,Rt}$, i.e. Stage D2, a small area at Point R4 exhibits a concentration of large surface principal strains with a maximum value at 1.1%.

c) As the applied force N_z increases, extensive plastic deformations are evident at Point R4, and large surface principal strains with a maximum value at 3.4% are developed in the junction when the applied force N_z reaches 920 kN or 1.0 $N_{z,Rt}$, i.e. Stage D3.

d) After the peak load is reached, unloading occurs in the T-joint. Local indentation with gross deformations in the chord takes place almost across the entire junction, i.e. from Point R4 towards Point R1 as well as towards R7. Hence, very large surface principal strains are obtained at all these points. The maximum surface principal strains at Point R4 are found to be 6.3% and 10.9% in Stages D4 and D5, respectively. It is apparent that the widths of the contours with a surface principal strain larger than 5.0% have been increased significantly, when compared with that in Stage D3.

Figure 21c) illustrates the surface principal compressive strains of various reference points at the welded junction of Joint T3 in various deformation stages, and it is shown that:

e) Point R4 always exhibits the largest surface principal strain while both Points R1 and R7 always exhibit the smallest.

f) The maximum surface principal strain of the junction under the peak load, i.e. Stage D3, is found to be 3.4% at Point R4 while the corresponding minimum surface principal strain is found to be 1.5% at Points R1 and R7.

g) After significant unloading, i.e. in Stage D5, the maximum and the minimum surface principal strains of the junction are found to be 10.9% at Point R4, and 6.8% at both Points R1 and R7 respectively.

Consequently, based on a detailed analysis on these precise measurements, the maximum surface principal compressive strain in these T-joints at failure is found to exceed 10.0%.

5.2 Deformation fields of Joint T11 under brace in-plane moments

Similar to above, Figure 22a) presents the surface principal tensile strain contours of Joint T11 at five deformation stages, namely Stages E1 to E5, together with the corresponding applied force-deformation curve in Figure 22b). It is evident that:

a) When the applied lateral force N_x is equal to 115 kN or 0.5 $N_{x,Rt}$, i.e. Stage E1, surface principal strains are found to be small in the junction though the maximum value is found to occur at Point R0, i.e. the crown point of the junction, at a value of 0.8 %. At Stage E2, which may be regarded as the point of proportional limit, the applied lateral force N_x is increased to 167 kN, or 0.7 $N_{x,Rt}$, and the maximum surface principal strain at Point R0 reaches 1.3 %.

b) As the applied lateral force $N_{j,x}$ increases, extensive plastic deformations are evident in the vicinity of Point R0. At Stages E3 and E4, large surface principal strains with a maximum value at 2.3 % and 4.3% are developed in the junction when the applied lateral force N_x reaches 192 kN or 0.8 $N_{x,Rt}$, and 217 kN or 0.9 $N_{x,Rt}$ respectively.

c) At Stage E5, the peak load at 230 kN is reached. After exhibition of a limited degree of ductility, a sudden fracture occurs in the vicinity of the heat-affect-zones of the welded junction. Hence, the maximum surface principal tensile strain is found to exceed 10.0%, and this is significantly larger than the expected strain at failure, i.e. 5.0%, in these joints recommended in Annex C of EN 1993-1-5[34].

Hence, an assessment on the surface principal strain contours at the welded junctions of both Joints T3 and T11 provides insights to the deformation characteristic of the T-joints in addition to various applied force-displacement curves of the T-joints presented in Sections 3 and 4. It provides a detailed picture on the development of plastic deformations of the welded junctions throughout the tests for an improved structural understanding on the failure mechanisms of the T-joints.

6 Design methods

The resistances of these T-joints under i) brace axial compression, and ii) brace in-plane moments are determined according to the design methods given in the following two design specifications:

6.1 Axial resistances of T-joints between CFCHS

Design Guide 1 of CIDECT

The design brace axial resistance of a T-joint between CHS against local chord plastification, $N_{z,Rd}$, is given by :

$$N_{z,Rd} = C_f \; Q_u \; Q_f \; \frac{f_{y0} t_0^2}{sin \, \theta_1} \tag{4a}$$

where

$$Q_u = 2.6 \; (1 + 6.8 \, \beta^2) \; \gamma^{0.2} \tag{4b}$$

$$Q_f = (1 - |n|)^{C_1} \tag{4c}$$

$$n = \frac{N_0}{N_{pl,0}} + \frac{M_0}{M_{pl,0}} \text{ in connecting face} \tag{4d}$$

where f_{y0} is the yield strength of the chord for S235 to S355 steels;
t_0 is the thickness of the chord ;
θ is the angle between the centrelines of the chord and of the brace ;
β is the ratio of brace diameter to chord diameter, i.e. $\beta = d_1 / d_0$;
γ is $d_0 / 2t_0$;
N_0 is the axial force applied to the chord ;
M_0 is the bending moment applied to the chord ;
$N_{pl,0}$ is the axial resistance of the chord ;
$M_{pl,0}$ is the plastic moment resistance of the chord ;
C_1 = 0.45 - 0.25 β for chord compression stress, i.e. $n < 0$; and
= 0.20 for chord tension stress, i.e. $n \geq 0$;

C_f is a reduction factor, and it is equal to 1.0 for S235 to S355 steels and 0.90 for S460 steels.

In the present investigation, it is proposed to adopt the above formula for design of T-joints between S690 CFCHS, and the same value of C_f , i.e. 0.90, is used.

EN 1993-1-8

The design brace axial resistance of a T-joint between CHS for local chord plastification, $N_{z,Rd}$, is given by:

$$N_{z,Rd} = C_f \; Q_u \; k_p \; \frac{f_{y0} t_0^2}{\sin \theta_1} \; / \; \gamma_{M5} \quad (5a)$$

$$Q_u = (2.8 + 14.2\beta^2) \; \gamma^{0.2} \quad (5b)$$

$$n_p = \frac{\sigma_{p,Ed}}{f_{y0}} \text{ in connecting face} \quad (5c)$$

where k_p = 1 - 0.3 n_p (1 + n_p) for n_p > 0 (compression);

k_p = 0 when n_p ≤ 0 (tension);

$\sigma_{p,Ed}$ is the maximum compressive stress in the chord excluding the stress due to components parallel to the chord axis ;

C_f is a reduction factor, and it is equal to 1.0 for S235 to S355 steels and 0.90 for S460 steels;

γ_{M5} is the partial safety factor for joints between structural hollow sections and it is taken as 1.0.

In the present investigation, it is proposed to adopt the above formula for design of T-joints between S690 CFCHS, but the value of C_f is taken to be 0.80 according to EN 1993:1-12 [35].

By adopting the measured dimensions and the measured yield strengths of the CFCHS given in Tables 2 and 6 respectively, the back analysis values of $N_{z,R}$ of the six T-joints according to both Design Guide 1 of CIDECT and EN 1993 are summarized in Table 7. A comparison on the back analysis values of the brace axial resistances reveals that

a) The ratios of $N_{z,Rt}$ / $N_{z,R}$ are found to range from 1.08 to 1.12 for those T-joints between S690 CFCHS, and 1.15 to 1.36 for those T-joints between S355 CFCHS according to Equation 4. Hence, the design method in Design Guide 1 of CIDECT is shown to be adequate for application to those T-joints between S690 CFCHS, though it is fairly conservative to those T-joints between S355 CFCHS.

   Similarly, the ratios of $N_{z,Rt}$ / $N_{z,R}$ are found to range from 1.36 to 1.46 for those T-joints between S690 CFCHS, and 1.48 to 1.55 for those T-joints between S355 CFCHS according to Equation 5. Hence, the design method in EN 1993-1-8 is also shown to be fairly conservative for application to those T-joints between S690 CFCHS as well as to those T-joints between S355 CFCHS.

b) In all T-joints between S690 CFCHS, i.e. Joints T2 and T3, and Joints T5 and T6, the ratios of the applied moments to the plastic moment resistances of the chords, $M_{j,Rt}$ / $M_{0,R}$, vary from 0.66 to 0.90, indicating that the full plastic moment resistances of the chords are not readily mobilized due to local chord plastification.

c) It is interesting to consider those two T-joints between S355 CFCHS, i.e. Joints T1 and T4, as follows:

- For Joint T1, owing to the presence of a brace with a relatively small diameter at 150 mm, the effect of chord plastificiation becomes critical. Hence, the full plastic moment resistance of the chord is not mobilized, and the ratio of the applied moment acting onto the chord to its plastic moment resistance, $M_{j,Rt}$ / $M_{0,R}$, is thus found to be 0.87.
- For Joint T4, owing to the presence of a brace with a relatively large diameter at 200 mm, the ratio of the applied moment acting onto the chord to its plastic moment resistance, $M_{j,Rt}$ / $M_{0,R}$, is found to be 1.05. Hence, the full plastic moment resistance of the chord is fully mobilized with a certain extent of strain hardening despite of an occurrence of local chord plastification.

It should be noted that in both design methods, there are reduction factors which consider the effect of co-existing (overall) bending moments and axial forces acting onto the chords, namely, Q_f in Design Guide 1 of CIDECT, and k_p in EN 1993-1-8. In these T-joints under brace axial compression, the applied forces cause large moments onto the chords, and these adverse effects are incorporated into the design methods through these reduction factors. The numerical values of these reduction factors Q_f and k_p for these T-joints are also presented in Table 7. As the values of Q_f and k_p are found to range from 0.64 to 0.79, these effects are considered to be very significant to the brace axial resistances of these T-joints.

6.2 Moment resistances of T-joints between CFCHS

Design Guide 1 of CIDECT

The design moment resistance of a T-joint between CHS against local chord plastification, $M_{j,Rd}$, is given by :

$$M_{j,Rd} = C_f\ Q_u\ Q_f\ \frac{f_{y0} t_0^2}{\sin\theta_1}\ d_1 \qquad (6a)$$

where

$$Q_u = 4.3\ \beta\ \gamma^{0.5} \qquad (6b)$$

$$Q_f = (1 - |n|)^{C_1} \qquad (6c)$$

$$n = \frac{N_0}{N_{pl,0}} + \frac{M_0}{M_{pl,0}} \text{ in connecting face} \qquad (6d)$$

The design moment resistance of a T-joint between CHS against chord punching shear, $M_{j,Rd}$, is given by :

$$M_{j,Rd} = C_f \, 0.58 \, f_{y0} \, t_0 d_1^2 \, \frac{1+3\sin\theta_1}{4\sin^2\theta_1} \qquad (6e)$$

where

C_f is a reduction factor which is equal to 1.0 for S235 to S355 steels, and 0.90 for S460 steels.

The design moment resistance of a T-joint between CHS against brace failure, $M_{j,Rd}$, is given by :

$$M_{j,Rd} = M_{1,Rd} \qquad (6f)$$

where

$M_{1,Rd}$ is the moment resistance of the brace according to EN1993-1-1[32].

Refer to Section 6.1 for definitions of the symbols.

In the present investigation, it is proposed to adopt the above formula for design of T-joints between S690 CFCHS, and the same value of C_f , i.e. 0.90, is used.

EN 1993-1-8

The design moment resistance of a T-joint between CHS against local chord plastification, $M_{j,Rd}$, is given by :

$$M_{j,Rd} = C_f \, 4.85 \, \frac{f_{y0} t_0^2}{\sin\theta_1} d_1 \sqrt{\gamma} \beta k_p \, / \, \gamma_{M5} \qquad (7a)$$

where

$$n_p = \frac{\sigma_{p,Ed}}{f_{y0}} \text{ in connecting face} \qquad (7b)$$

Moreover, the design moment resistance of a T-joint between CHS against chord punching shear, $M_{j,Rd}$, is given by :

$$M_{j,Rd} = C_f \, \frac{f_{y0} t_0 d_1^2}{\sqrt{3}} \, \frac{1+3\sin\theta_1}{4\sin^2\theta_1} \, / \, \gamma_{M5} \qquad (7c)$$

C_f is a reduction factor which is equal to 1.0 for S235 to S355 steels, and 0.90 for S460 steels.

γ_{M5} is the partial safety factor for joints between structural hollow sections and it is taken as 1.0.

Refer to Section 6.1 for definitions of the symbols.

In the present investigation, it is proposed to adopt the above formula for design of T-joints between S690 CFCHS, but the value of C_f is taken to be 0.80 according to EN 1993:1-12 [35].

By adopting the measured dimensions and the measured yield strengths of the CFCHS given in Tables 2 and 6 respectively, the values of $M_{j,R}$ of the six T-joints according to both Design Guide 1 of CIDECT and EN 1993 against i) chord plastification, ii) chord punching shear failure, and iii) brace failure are summarized in Table 8. It should be noted that although Braces BR01 and BR02 are merely classified as Class 3 or 4 sections according to the current design rules on section classification, their plastic moment resistances are demonstrated to be fully mobilized at their braces in the tests as they are properly welded onto the supporting chords. Hence, their plastic moment resistances are adopted in the back analyses. A comparison on the back analysis values of the brace moment resistances reveals that

- Series Q1 – 150/250: Joints T7, T8 and T9 under brace in-plane moments

  For Joint T7 (d_1 = 150 and t_1 = 6 mm), i.e. a T-joint between S355 CFCHS, the back analysis value of the brace moment resistance is 46.2 kNm which is smaller than the joint moment resistances due to i) chord plastification at 49.9 kNm, and ii) chord punching shear failure at 47.6 kNm. This agrees with the observed mode of failure, i.e. brace failure.

  For Joints T8 and T9 (both d_1 = 150 and t_1 = 6 mm), i.e. both T-joints between S690 CFCHS, the back analysis value of the joint moment resistance due to punching shear failure is 90.0 kNm which is smaller than the joint moment resistances due to i) chord plastification at 94.3 kNm, and ii) brace failure at 93.0 kNm. However, it should be noted that the difference among these moment resistances is merely 3.0 kNm, i.e. 3.3%, and hence, these T-joints deform towards a combined failure mode of chord plastification and brace failure.

- Series Q2 – 200/250: Joints T10, T11 and T12 under brace in-plane moments

  For Joint T10 (d_1 = 200 and t_1 = 6 mm), i.e. a T-joint between S355 CFCHS, the back analysis value of the brace moment resistance is 83.8 kNm which is smaller than the joint moment resistance due to i) chord plastification at 88.8 kNm, and ii) chord punching shear failure at 84.7 kNm. This agrees with the observed mode of failure, i.e. brace failure.

  For Joint T11 (d_1 = 200 and t_1 = 6 mm), i.e. a T-joint between S690 CFCHS, the back analysis value of the joint moment resistance due to chord punching shear failure is 159.9 kNm which is marginally larger than the joint moment resistances due to i) chord plastification at 167.7 kNm, and ii) brace failure at 168.3 kNm. However, this does not agree with the observed mode of failure, i.e. brace failure. Nevertheless, the difference among these moment resistances is merely 8.4 kNm, i.e. 5.3%, and these T-joints deform towards a combined failure mode of chord plastification and brace failure.
  Hence, a combined failure mode is considered to occur in Joints T10 and T11.

  For Joint T12 (d_1 = 200 and t_1 = 10 mm), i.e. a T-joint between S690 CFCHS, the back analysis value of the joint moment resistance due to chord punching shear failure is 159.9 kNm which is marginally larger than the joint moment resistances due to i) chord plastification at 167.7 kNm, and ii) brace failure at 269.2 kNm. This agrees with the observed mode of failure, i.e. chord punching shear failure, though significant plastic deformations in the chord are also apparent.

Hence, after a careful examination into various moment resistances of these joints, two modes of failure are identified, and effectiveness of the current design methods is assessed. It should be noted that:

- Brace failure in both T-joints between S355 CFCHS, i.e. Joints T7 and T10, is readily predicted with the use of the current design rules.

- Both chord punching shear failure and brace failure in those T-joints between S690 CFCHS, i.e. Joints T8 and T9 as well as T11 and T12, are readily predicted with the use of the current design rules. The back analysis values of the moment resistances of these competing modes of failure are found to be very close to one another as they differ merely by 3.3 to 5.3%.

- Section classification rules for S690 CFCHS should be improved, and their plastic moment resistances should be fully mobilized at their bases when they are properly welded onto the supporting chords.

7. Conclusions

This paper reports an experimental investigation into the structural behaviour of T-joints between S690 cold-formed circular hollow sections (CFCHS). A total of twelve T-joints of both S355 and S690 CFCHS under *i) brace axial compression*, and *ii) brace in-plane moments* are tested to failure in order to examine their deformation characteristics, in particular, their joint resistances and failure modes. These tests are conducted with extensive instrumentation on both overall deformations of the T-joints and local deformations of their welded brace/chord junctions. Welding of all of these T-joints between S690 CFCHS are carefully performed so that the heat input energy during welding vary narrowly between 1.2 and 1.5 kJ/mm. Standard tensile tests are also conducted on both flat and curved coupons extracted from the sections to provide mechanical properties for subsequent strength analysis.

After a careful data analysis and interpretation on both the measured and the design resistances of the T-joints, the following conclusions are drawn:

a) For those T-joints under brace axial compression, they are found to fail primarily in local chord plastification together with local indentation and overall bending in the chords. The maximum surface principal *compressive* strains measured in typical T-joints between S690 CFCHS are found to exceed 10.0 %. Nevertheless, structural benefits due to an increase in yield strengths, i.e. from S355 steels to S690 steels, cannot be fully mobilized in these T-joints between S690 CFCHS because of a reduced strain hardening.

b) For those T-joints between S690 CFCHS under brace in-plane moments, both brace failure with HAZ fracture at the welded brace bases and chord punching shear failure are found to be critical. It is evident that the plastic moment resistances of these braces are fully mobilized, but they exhibit a reduced ductility, when compared with those T-joints between S355 CFCHS. Nevertheless, the maximum surface tensile principal strains measured in typical T-joints between S690 CFCHS are also found to exceed 10.0 %.

c) The measured resistances of those T-joints between S690 CFCHS under i) brace axial compression, and ii) brace in-plane moments are found to be adequately predicted with the current design rules given in Design Guide 1 of CIDECT and EN 1993 with an appropriate choice of the parameter C_f . This is clearly demonstrated in the back analyses of the design rules with measured yield strengths of the S690 CFCHS.

Consequently, it is established in this experimental investigation that the effects of welding onto the mechanical properties of the S690 welded sections as well as the structural behaviour of these T-joints are shown to be significantly less pronounced than generally anticipated, provided that the welding processes and parameters are properly controlled. Moreover, this investigation provides structural insights and scientific data for possible improvements onto prediction capabilities of the design methods. It is also recommended to establish advanced finite element models to predict the resistances of the T-joints between S690 CFCHS under i) brace axial compression, and ii) brace in-plane moments over a wide range of cross-sectional dimensions. The models will be carefully calibrated against the experimental data of the present study, and this will be reported separately.

Acknowledgments

The authors are grateful for the financial support provided by the Research Grants Council of the Government of Hong Kong SAR (Project Nos. PolyU 152194/15E, 1526871/16E, 152231/17E and 152157/18E). The project leading to the publication of this paper was also partially funded by the Research Committee (Project No. RTZX and RJLY) and the Chinese National Engineering Research Centre for Steel Construction (Hong Kong Branch) (Project No. 1-BBY3 & 6) of the Innovation and Technology Fund and the Hong Kong Polytechnic University. Special thanks go to the Nanjing Iron and Steel Company Ltd. in Nanjing, the Pristine Steel Fabrication Company Ltd. in Dongguan, and the Industrial Centre of the Hong Kong Polytechnic University.

REFERENCES

[1] Wardenier, J., Packer, J. A., Zhao, X. L. and Van der Vegte, G. J. (2002). Hollow sections in structural applications. Rotterdam,, The Netherlands: Bouwen met staal.

[2] Wardenier, J., Kurobane, Y., Packer, J. A., Van der Vegte, G. J. and Zhao X. L. (2008). Design guide for circular hollow section (CHS) joints under predominantly static loading. CIDECT.

[3] CEN. (2005). EN 1993-1-8: Design of steel structures Part 1-8: Design of joints. European Committee for Standardization.

[4] International Institute of Welding (IIW). (1981). Design recommendations for hollow section joints — predominantly statically loaded. IIW Doc. XV-701-89. 1st edition.

[5] International Institute of Welding (IIW). (1989). Design recommendations for hollow section joints — predominantly statically loaded. IIW Doc. XV-701-89. 2nd edition.

[6] International Institute of Welding (IIW). (2009). Design recommendations for hollow section joints — predominantly statically loaded. IIW Doc. XV-701-89. 3rd edition.

[7] Choi, B. J., Lee, E. T., Yang, J. G. and Kang, C. K. (2012). Axial capacity of circular hollow section T-joints using grade HSB 600 steel. International Journal of Steel Structures, 12(4): 483-494.

[8] Kim, J. W., Kim, S. S., Lee, M. J. and Yang, J. G. (2012). Vierendeel joints in the circular hollow sections of high strength steel subjected to brace moment and chord compressive loadings. International Journal of Steel Structures, 12(4): 579-587.

[9] Qian, X. D., Choo, Y. S., Van Der Vegte, G. J. and Wardenier, J. (2008). Evaluation of the new IIW CHS strength formulae for thick-walled joints. In Proceedings of the Twelfth International Symposium on Tubular Structures, Shanghai. Taylor & Francis, London, pp271-280.

[10] Vegte, G. V. D., Wardenier, J., Zhao, X. L. and Packer, J. A. (2009) Evaluation of new CHS strength formulae to design strengths. Proceedings of 12th International Symposium on Tubular Structures, Shanghai, China, pp. 313–322.

[11] Havula, J., Garifullin, M., Heinisuo, M., Mela, K., & Pajunen, S. (2018). Moment-rotation behaviour of welded tubular high strength steel T joint. Engineering Structures, 172, 523-537.

[12] Pandey, M., & Young, B. (2019). Compression capacities of cold-formed high strength steel tubular T-joints. Journal of Constructional Steel Research, 162, 105650.

[13] Pandey, M., & Young, B. (2019). Tests of cold-formed high strength steel tubular T-joints. Thin-Walled Structures, 143, 106200.

[14] Pandey, M., & Young, B. (2020). Structural performance of cold-formed high strength steel tubular X-Joints under brace axial compression. Engineering Structures, 109768.

[15] Lan, X., Chan, T. M., & Young, B. (2019). Structural behaviour and design of high strength steel RHS X-joints. Engineering Structures, 200, 109494.

[16] Lan, X., Chan, T. M., & Young, B. (2020). Experimental study on the behaviour and strength of high strength steel CHS T-and X-joints. Engineering Structures, 206, 110182.

[17] Becque, J. and Wilkinson, T. (2017). The capacity of grade C450 cold-formed rectangular hollow section T and X connections: An experimental investigation. Journal of Constructional Steel Research, 133: 345-359.

[18] Lee, C. H., Kim, S. H., Chung, D. H., Kim, D. K. and Kim, J. W. (2017). Experimental and numerical study of cold-formed high-strength steel CHS X-joints. Journal of Structural Engineering, 143(8), 04017077.

[19] Ho, H.C., Chung, K.F., Huang, M.X., Nethercot, D.A., Liu, X., Hao, J., Wang, G.D. and Tian, Z.H. (2020). Mechanical properties of high strength S690 steel welded sections

through tensile tests on heat-treated coupons, Journal of Constructional Steel Research, 166: 105922.

[20] Liu, X., Chung, K. F., Ho, H. C., Xiao, M., Hou, Z. X. and Nethercot, D. A. (2018). Mechanical behavior of high strength S690-QT steel welded sections with various heat input energy. Engineering Structures, 175: 245-256.

[21] Hu, Y. F. and Chung, K. F. (2017). Numerical study on residual stresses in high strength Q690 cold-formed circular hollow sections, Proceedings of the Fifteenth East Asia-Pacific Conference on Structural Engineering and Construction (EASEC 15), October 2017, pp910-917.

[22] Hu, Y. F., Chung, K. F., Ban, H., & Nethercot, D. A. (2020). Investigations into residual stresses in S690 cold-formed circular hollow sections due to transverse bending and longitudinal welding. Engineering Structures, 219, 110911.

[23] Hu, Y. F. and Chung, K. F. (2018). Structural tests on high strength S690 steel CHS T-joints subjected to in-plane bending. Proceedings of the International Conference on Engineering Research and Practice for Steel Construction 2018 (ICSC 2018), September 2018, pp715-720.

[24] Hu, Y. F. (2019). Structural behavior of high strength S690 steel cold-formed circular hollow sections, Doctoral dissertation, the Hong Kong Polytechnic University. Hong Kong SAR.

[25] Li, J., Dan, X., Xu, W., Wang, Y., Yang, G. and Yang, L. (2017). 3D digital image correlation using single color camera pseudo-stereo system. Optics & Laser Technology, 95, 1-7.

[26] Ho, H. C., Chung, K. F., Liu, X., Xiao, M. and Nethercot, D. A. (2019). Modelling tensile tests on high strength S690 steel materials undergoing large deformations. Engineering Structures, 192: 305-322.

[27] AWS (1995) Specification for Carbon Steel Electrodes for Flux Cored Arc Welding. Structural Welding Code – Steel. Miami, United States: American Welding Society.

[28] AWS (2005) Specification for Low-Alloy Steel Electrodes and Rods for Gas Shielded Arc Welding. Structural Welding Code – Steel. Miami, United States: American Welding Society.

[29] Chung, K. F., Ho, H. C., Hu, Y. F., Wang, K., Liu, X., Xiao, M., & Nethercot, D. A. (2020). Experimental evidence on structural adequacy of high strength S690 steel welded joints with different heat input energy. Engineering Structures, 204, 110051.

[30] Garifullin, M., Launert, B., Heinisuo, M., Pasternak, H., Mela, K. and Pajunen, S. (2018), "Effect of welding residual stresses on local behavior of rectangular hollow section joints - Part 1- Development of numerical model", Bauingenieur, 93, 152-159.

[31] BS EN ISO 6892-1 (2009). Metallic materials – Tensile testing: Part 1: Method of test at ambient temperature, British Standards Institution.

[32] CEN. (2005). EN 1993-1-1: Design of steel structures. Part 1-1: General rules and rules for buildings. European Committee for Standardization.

[33] Lu, L. H., De Winkel, G. D., Yu, Y. and Wardenier, J. (1994). Deformation limit for the ultimate strength of hollow section joints. The Sixth International Symposium on Tubular Structures, pp341-347.

[34] CEN. (2005). EN 1993-1-5: Design of steel structures. Part 1-1: Plated structural elements. European Committee for Standardization.

[35] CEN. (2007). BS EN 1993-1-12: Design of steel structures. Part 1-12: Additional rules for the extension of EN 1993 up to steel grades S700. European Committee for Standardization.

Figure 1 Application of tubular T-joints in Vierendeel trusses

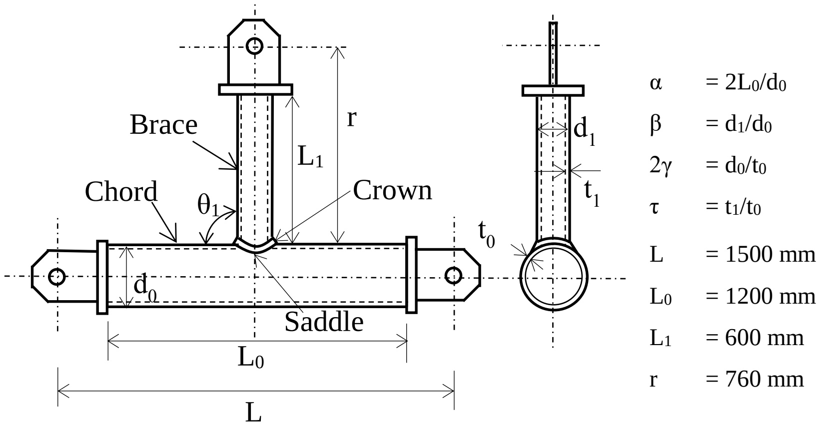

Figure 2 Overall configuration of a typical T-joint

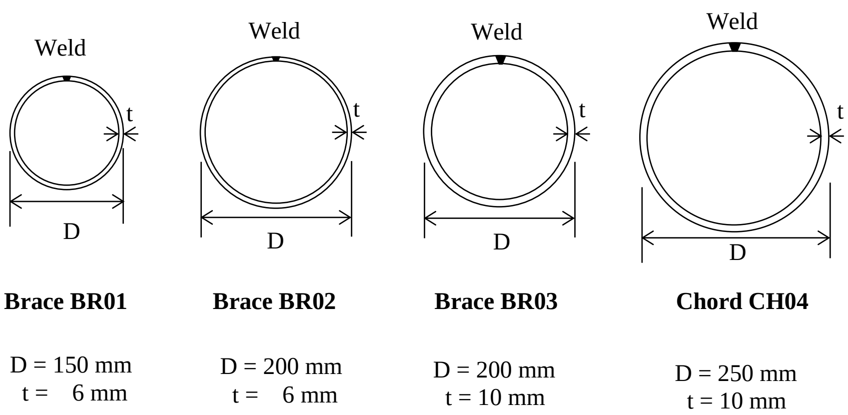

Figure 3 Nominal sectional dimensions of CFCHS

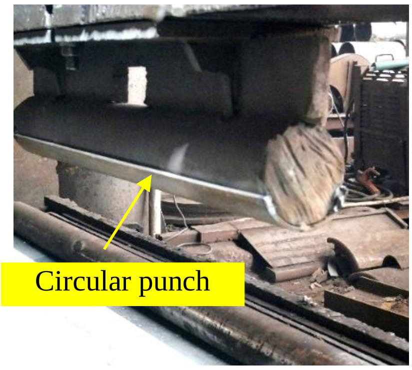

a) Press-braking of plate edges

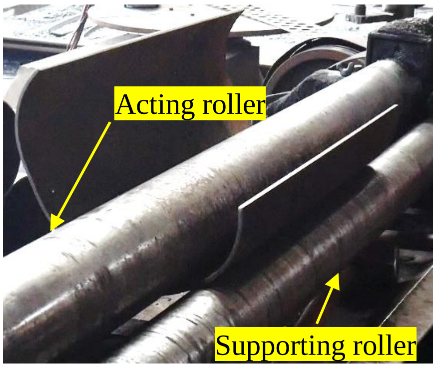

b) Transverse bending with three rollers

c) Longitudinal welding after transverse bending

d) Welding quality at the brace-chord junction

Figure 4 Fabrication process of welded CFCHS

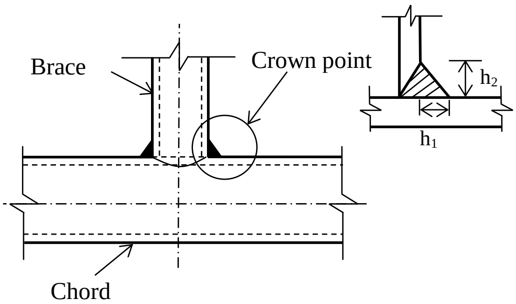

a) Crown point

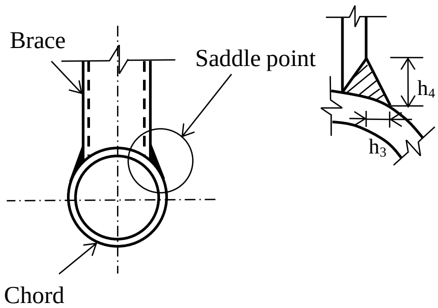

b) Saddle point

Figure 5 Welding details of T-joints

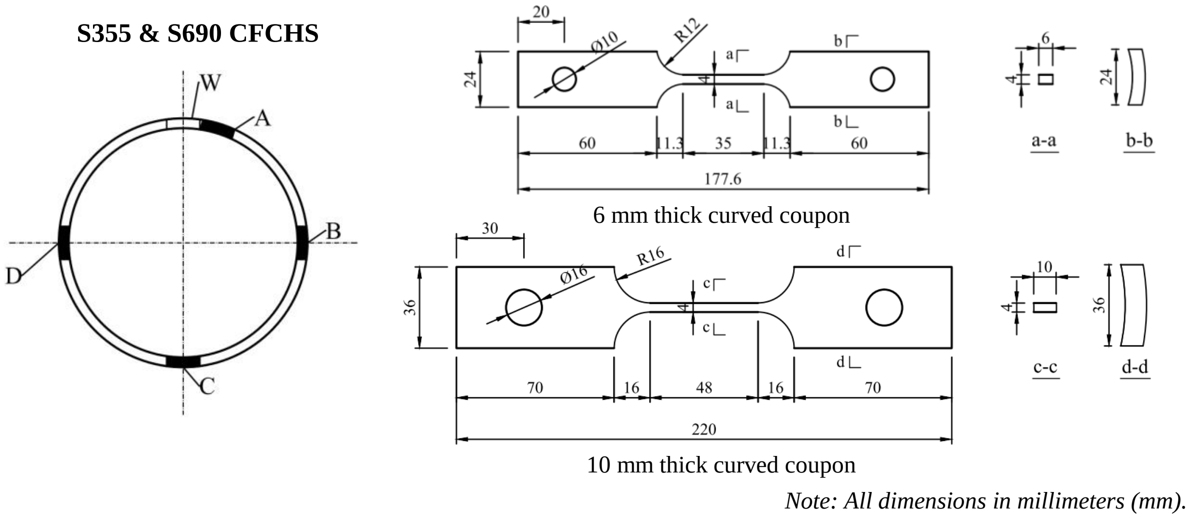

Figure 6 Typical locations and geometric dimensions of curved coupons

a) Test setup

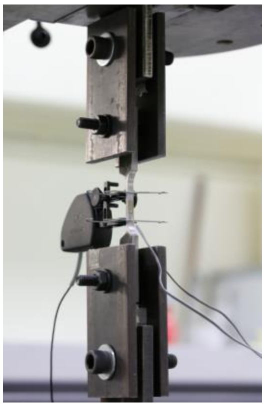

b) A curved coupon under testing

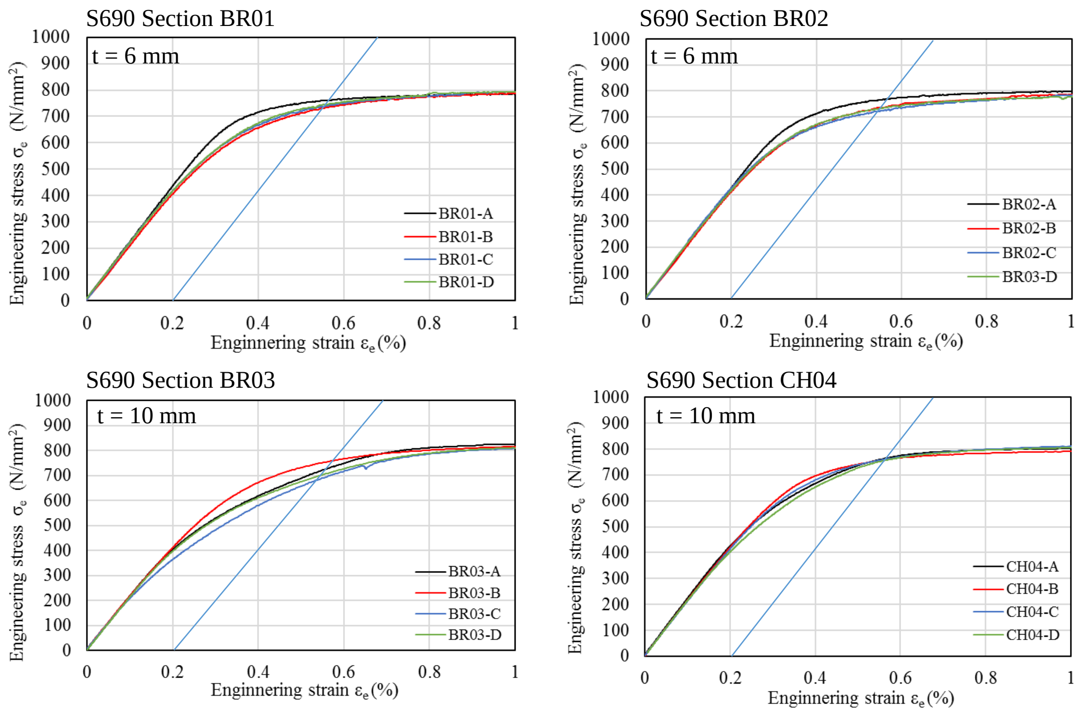

c) Engineering stress-strain curves of curved coupons

Figure 7 Tensile tests on curved coupons

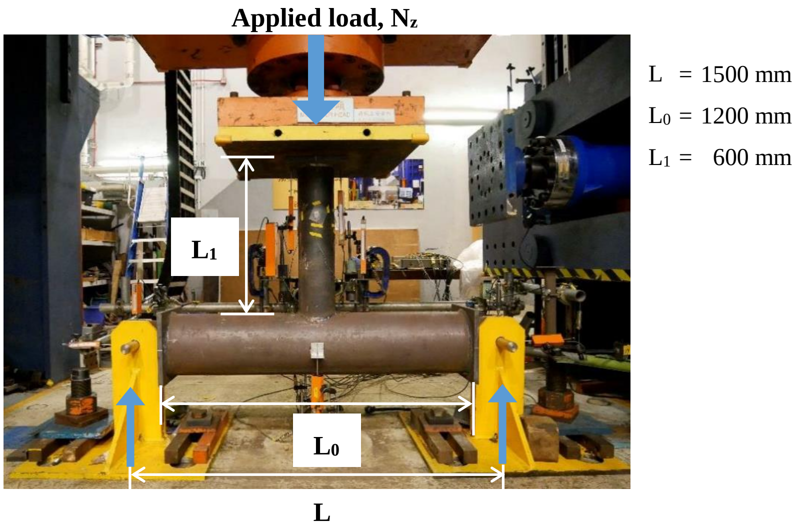

a) Overall arrangement

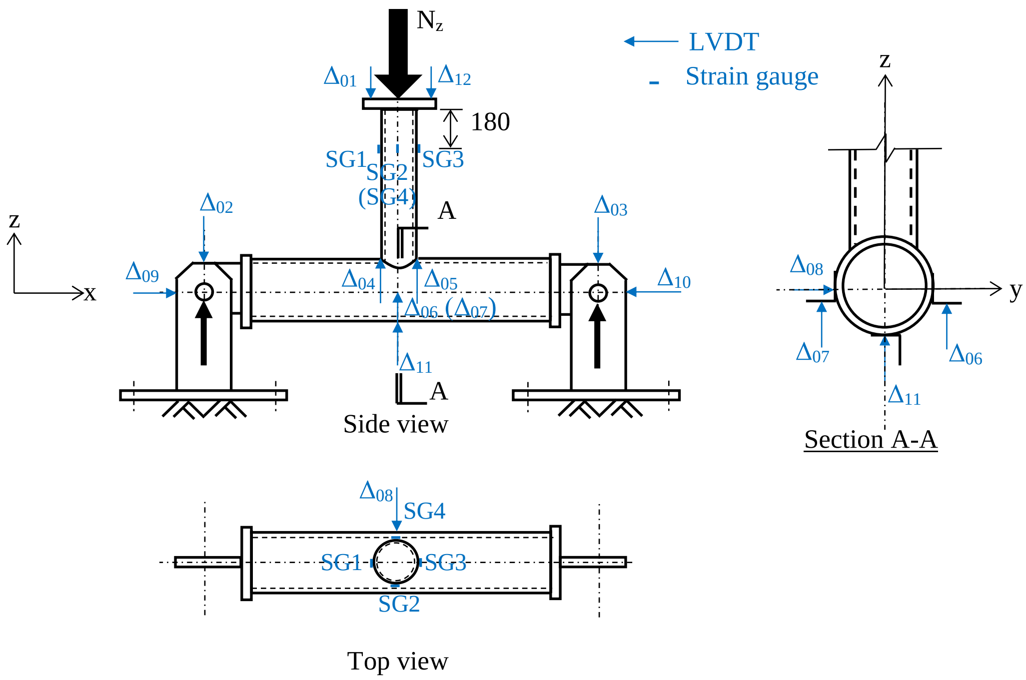

b) Instrumentation

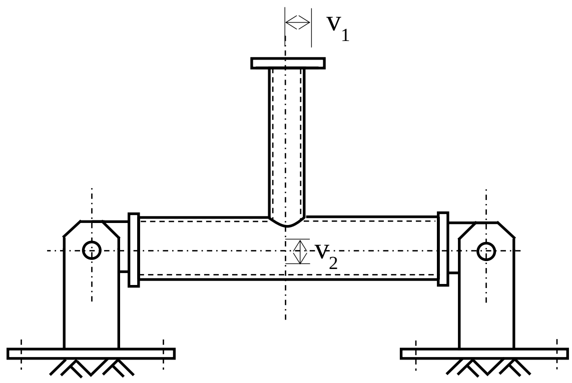

c) Initial out-of-straightness

Figure 8 Compression tests on T-joints between CFCHS

Joint T1

Joint T2

Joint	Steel grade	Chord $d_0 \times t_0$ (mm×mm)	Brace $d_1 \times t_1$ (mm×mm)
T1	S355	250×10	150×6
T2	S690	250×10	150×6
T3		250×10	150×6

Joint T3

Joint T4

Joint T5

Joint	Steel grade	Chord $d_0 \times t_0$ (mm×mm)	Brace $d_1 \times t_1$ (mm×mm)
T4	S355	250×10	200×6
T5	S690	250×10	200×6
T6		250×10	200×10

Joint T6

Note: All T-joints exhibit significant chord failure under i) overall plastic bending, and ii) local chord plastification.

Figure 9 Deformed T-joints under brace axial compression after tests

a) Plastic deformation at crown point

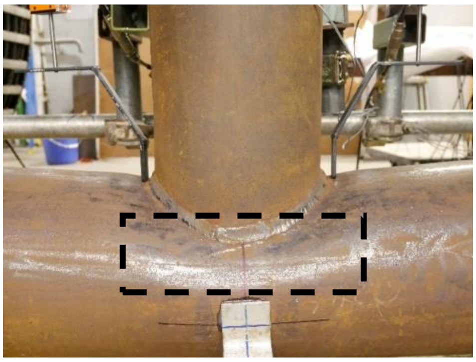

b) Plastic deformation at saddle point

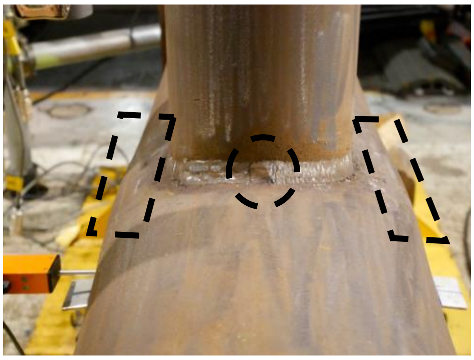

c) Local chord plastification

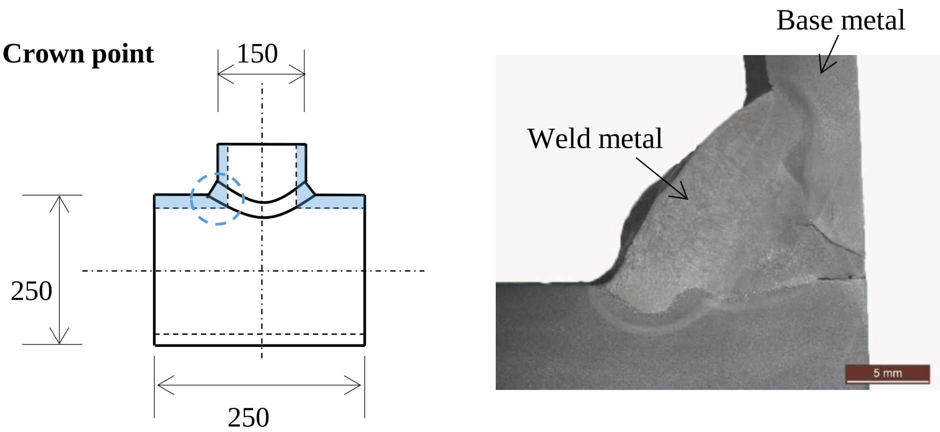

d) Typical detail of a welded connection — Joint T3

Figure 10 Typical failure modes of T-joints under brace axial compression

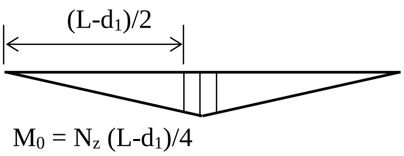

a) Bending moment diagram

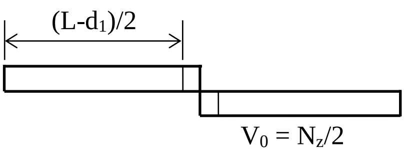

b) Shear force diagram

Figure 11 Internal forces of the chord in a typical T-joint

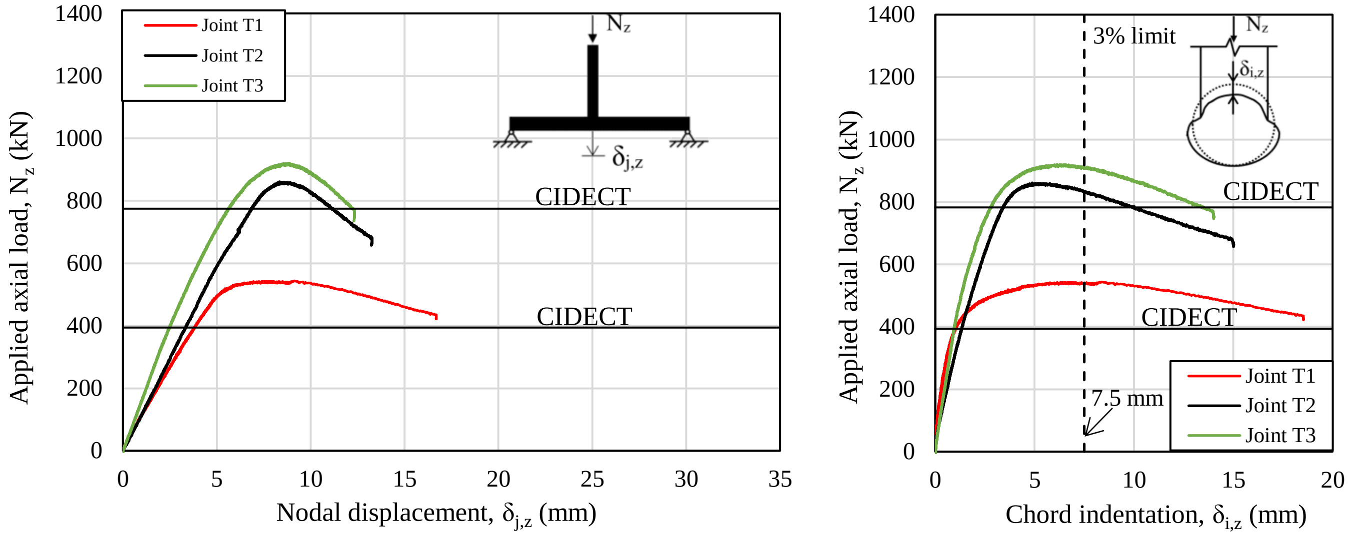

Series P1-150/250

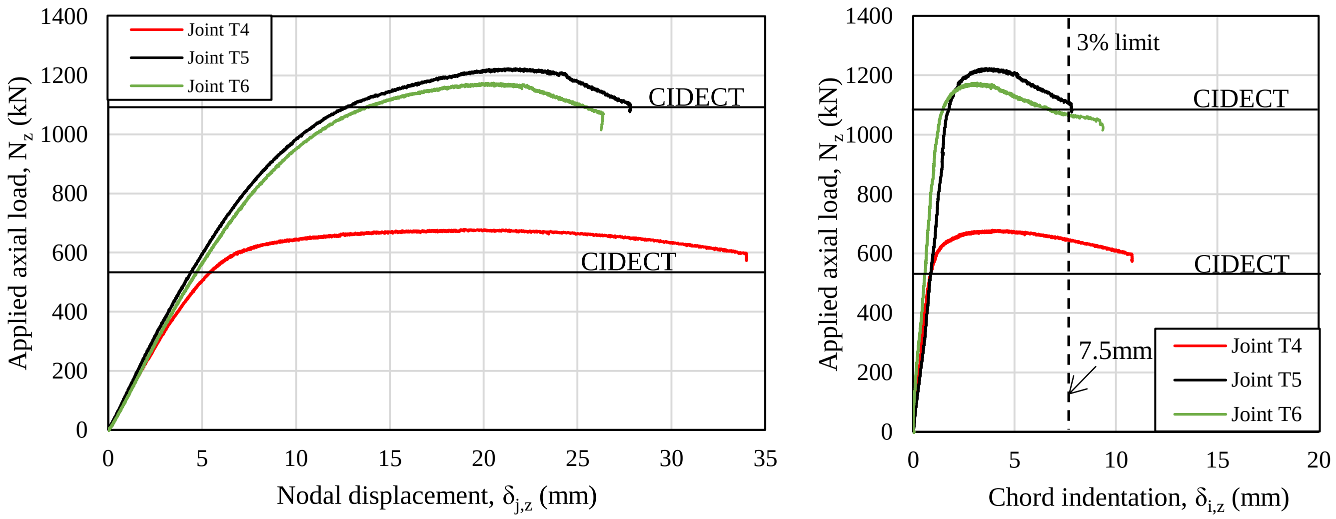

Series P2-200/250

a) Applied load-joint nodal displacement curves

b) Applied load-chord indentation curves

Figure 12 Measured load-deformation curves of T-joints

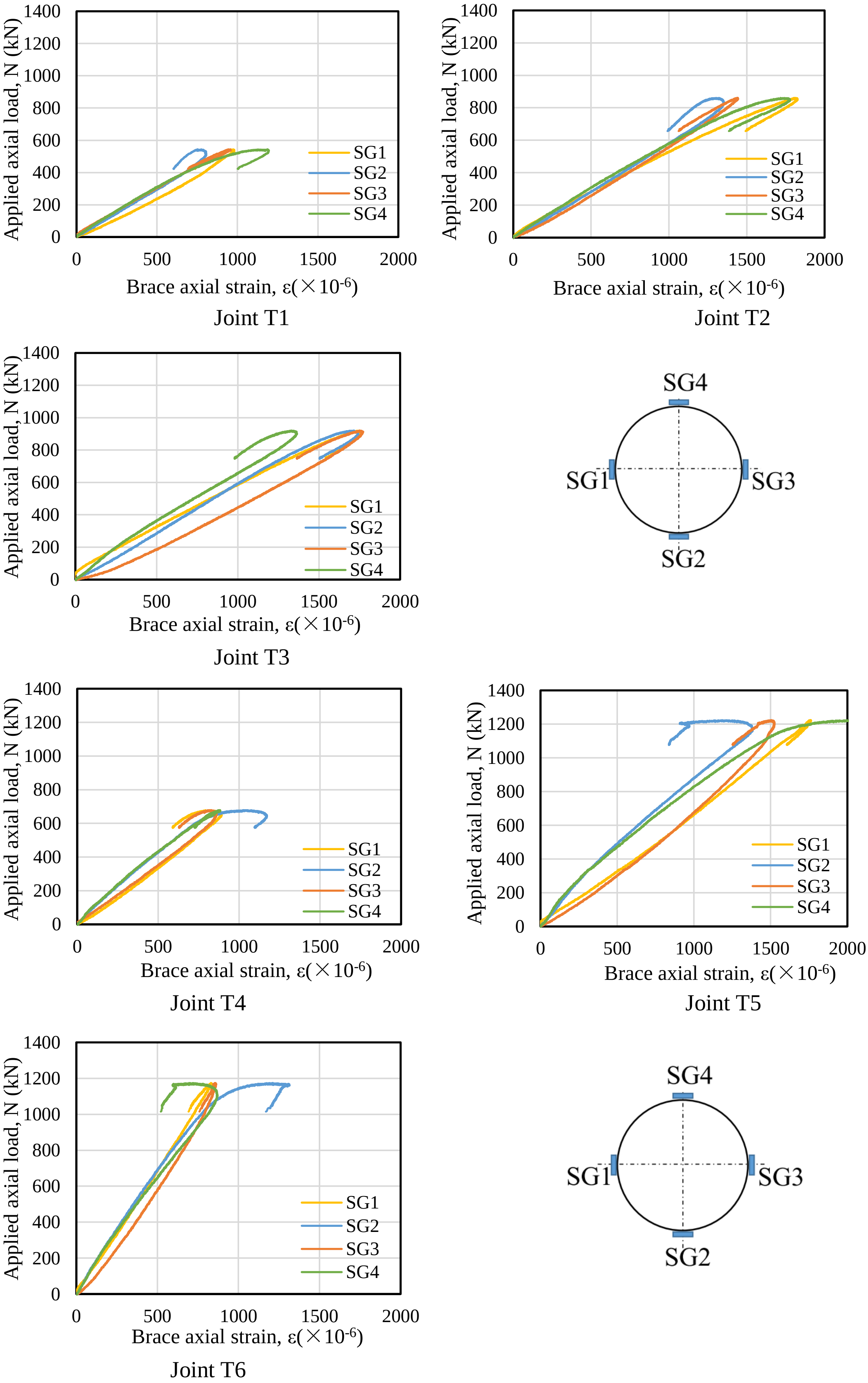

Figure 13 Applied load - brace axial strain curves

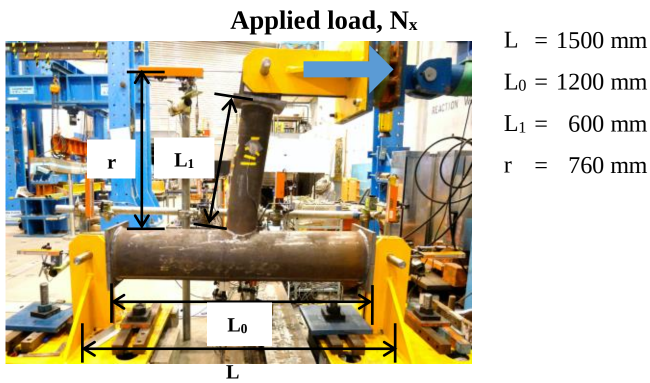

a) Test set-up

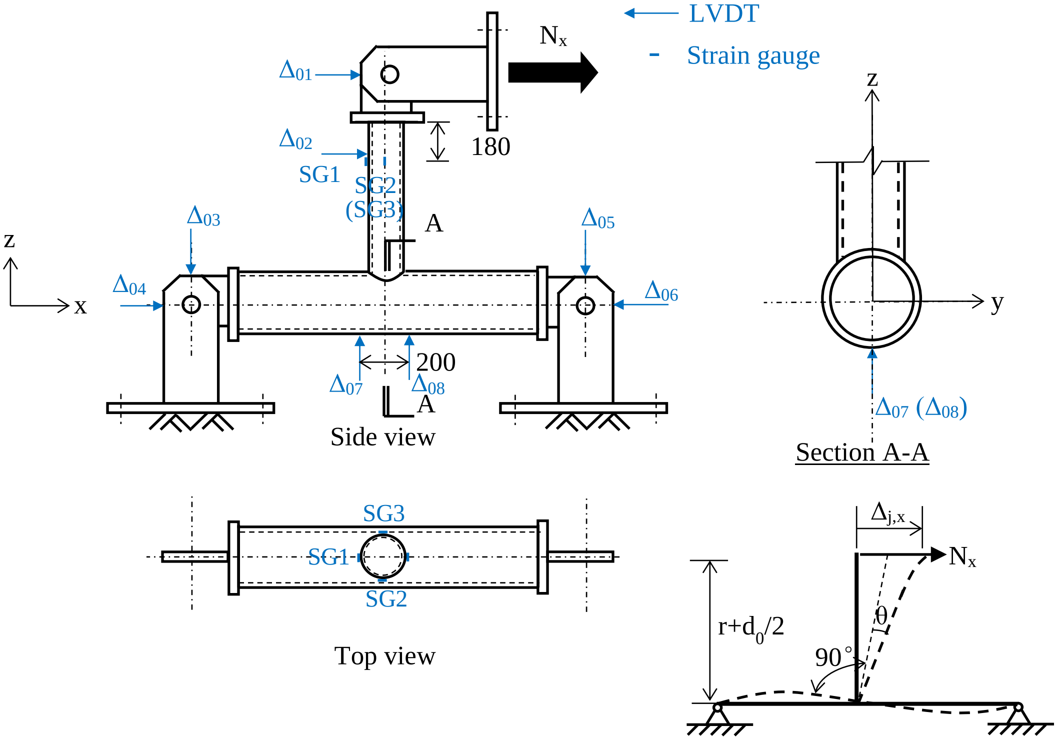

b) Instrumentation

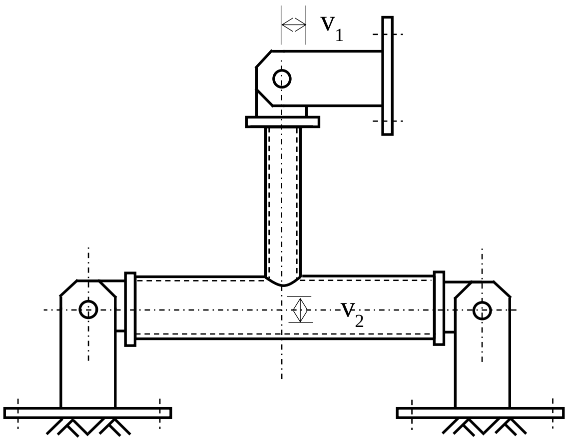

c) Initial out-of-straightness

Figure 14 In-plane bending tests on T-joints between CFCHS

Joint T7

Joint T8

Joint	Steel grade	Chord $d_0 \times t_0$ (mm×mm)	Brace $d_1 \times t_1$ (mm×mm)
T7	S355	250×10	150×6
T8	S690	250×10	150×6
T9		250×10	150×6

Joint T9

Joint T10

Joint T11

Joint	Steel grade	Chord $d_0 \times t_0$ (mm×mm)	Brace $d_1 \times t_1$ (mm×mm)
T10	S355	250×10	200×6
T11	S690	250×10	200×6
T12		250×10	200×10

Joint T12

Figure 15 Deformed T-joints under brace in-plane bending after tests

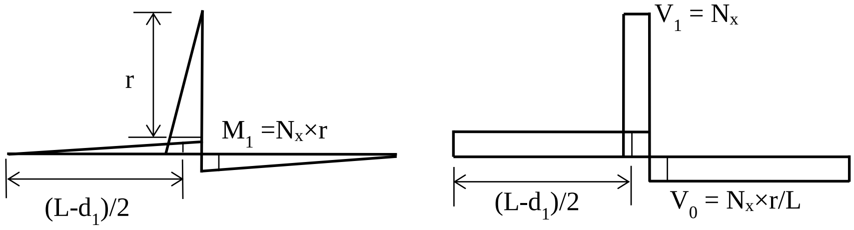

a) Bending moment diagram b) Shear force diagram

Figure 16 Internal forces of a T-joint under in-plane bending

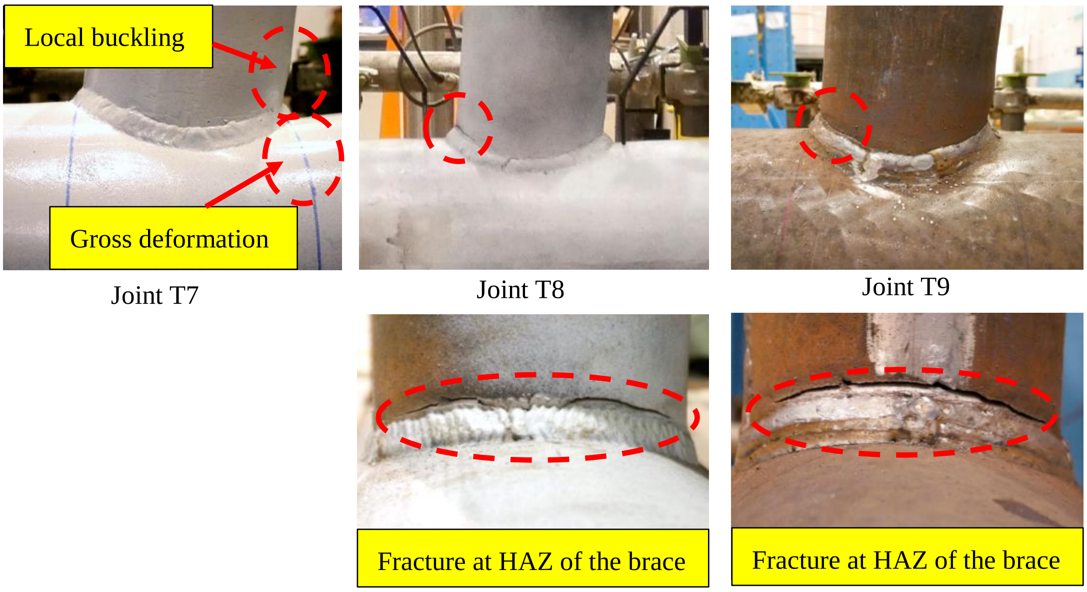

a) Typical failure modes of T-joints under brace in-plane bending

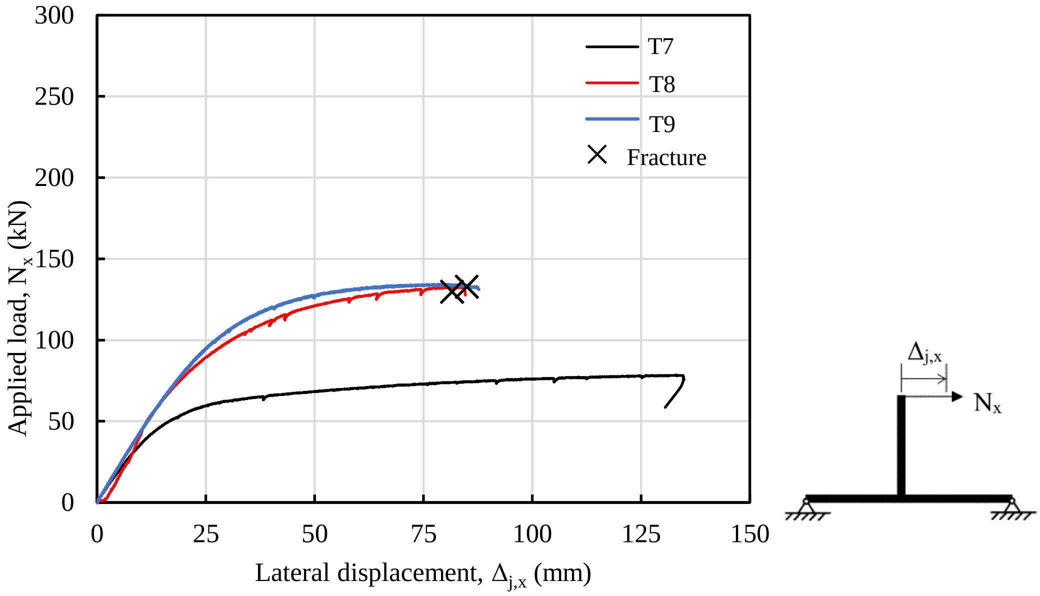

Series Q1-150/250

b) Lateral load-lateral displacement curves of T-joints under brace in-plane bending

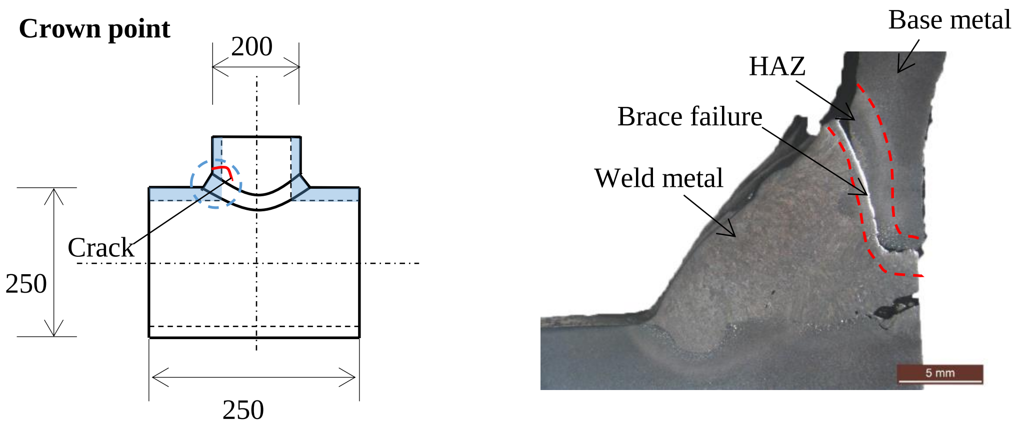

c) Typical detail of a welded connection after etching — Joint T11

Figure 17 Test results for Series Q1

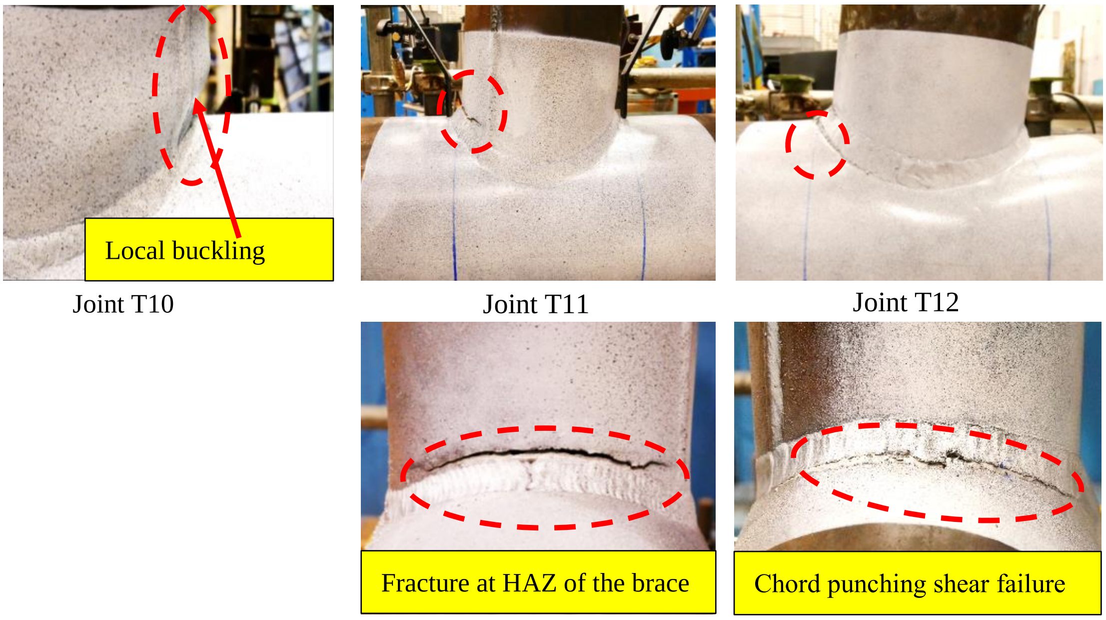

a) Typical failure modes of T-joints under brace in-plane bending

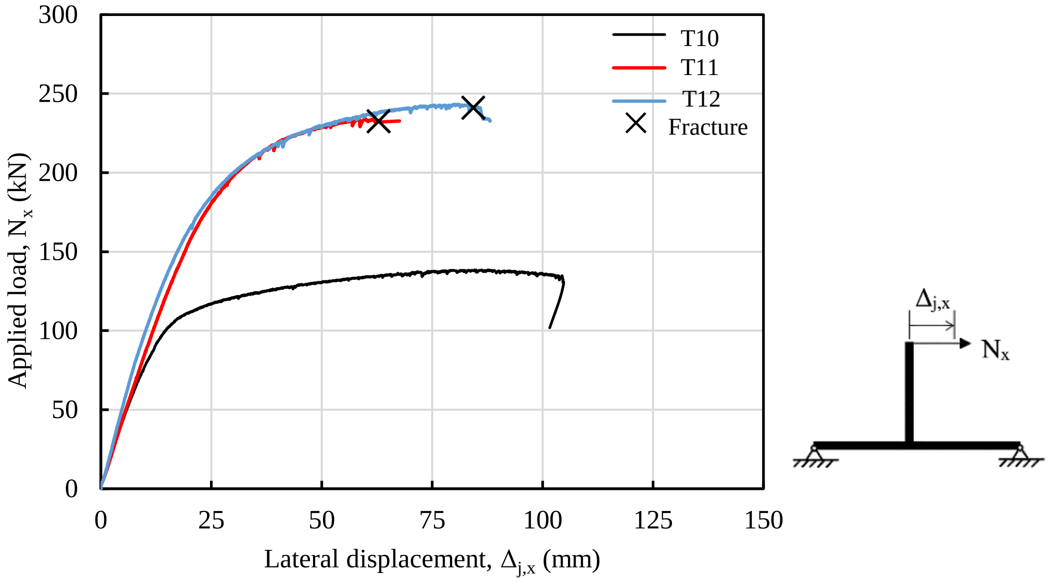

Series Q2-200/250

b) Lateral load-lateral displacement curves of T-joints under brace in-plane bending

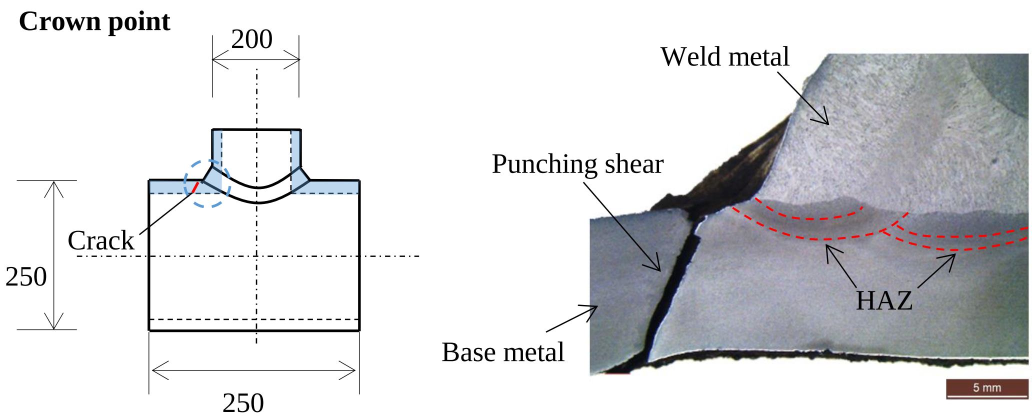

c) Typical detail of a welded connection after etching — Joint T12

Figure 18 Test results for Series Q2

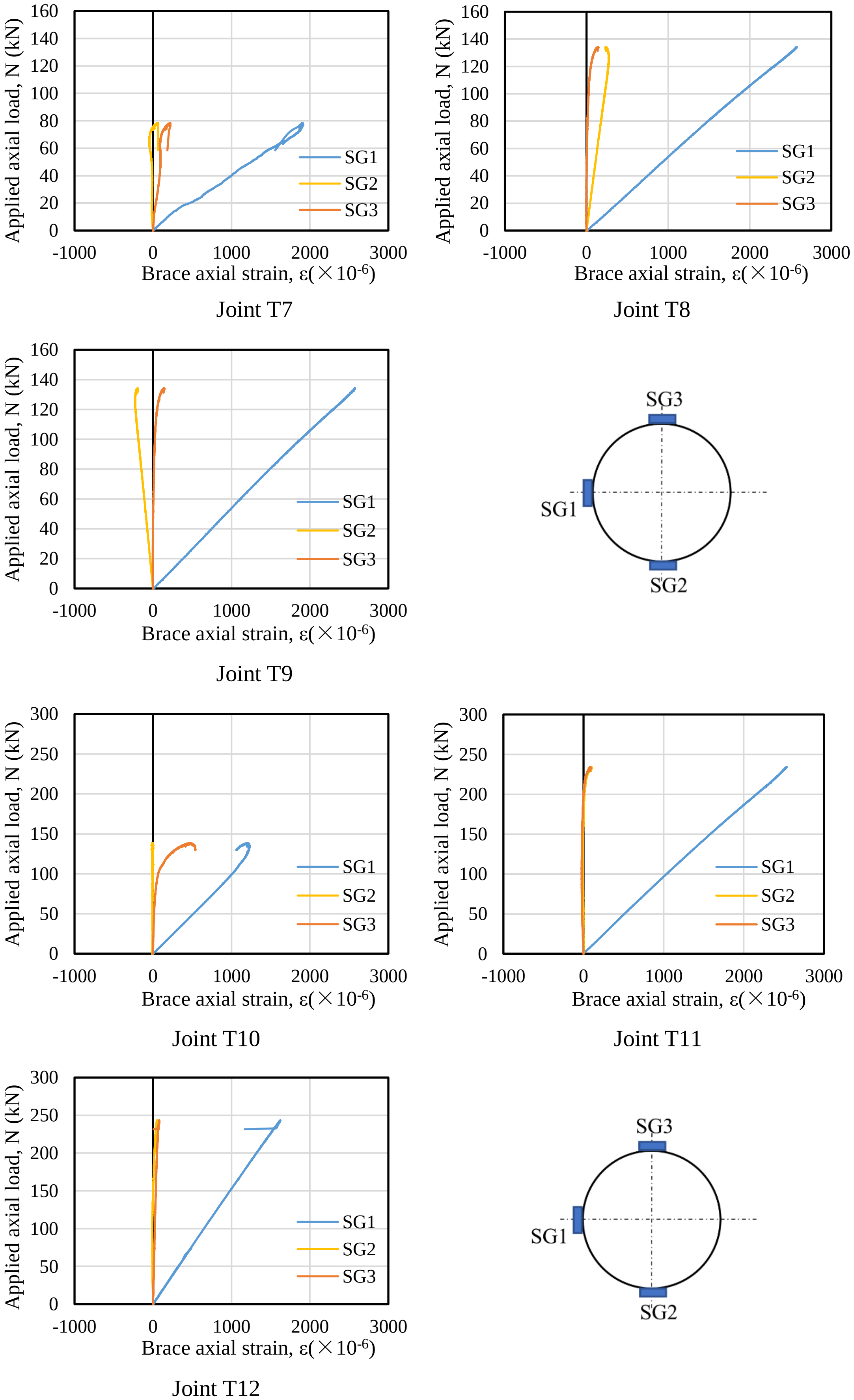

Figure 19 Applied load - brace axial strain curves

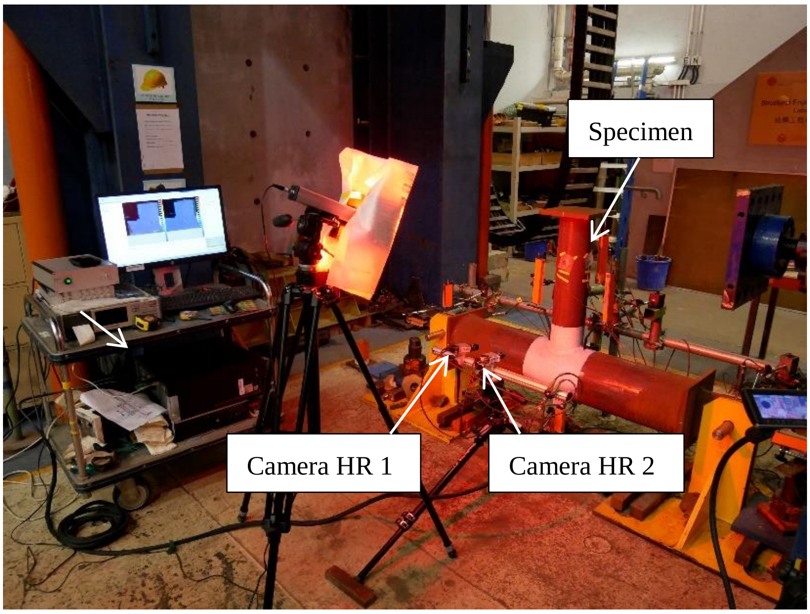

a) Test set-up

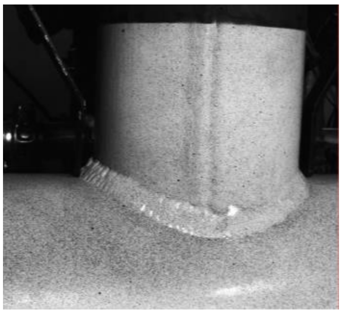

Camera HR 1

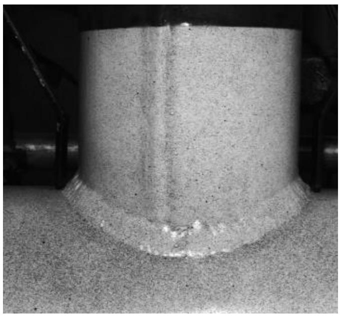

Camera HR 2

b) High resolution images at 5M pixels

Figure 20 Set-up of DIC system for non-contact measurements of surface deformation fields

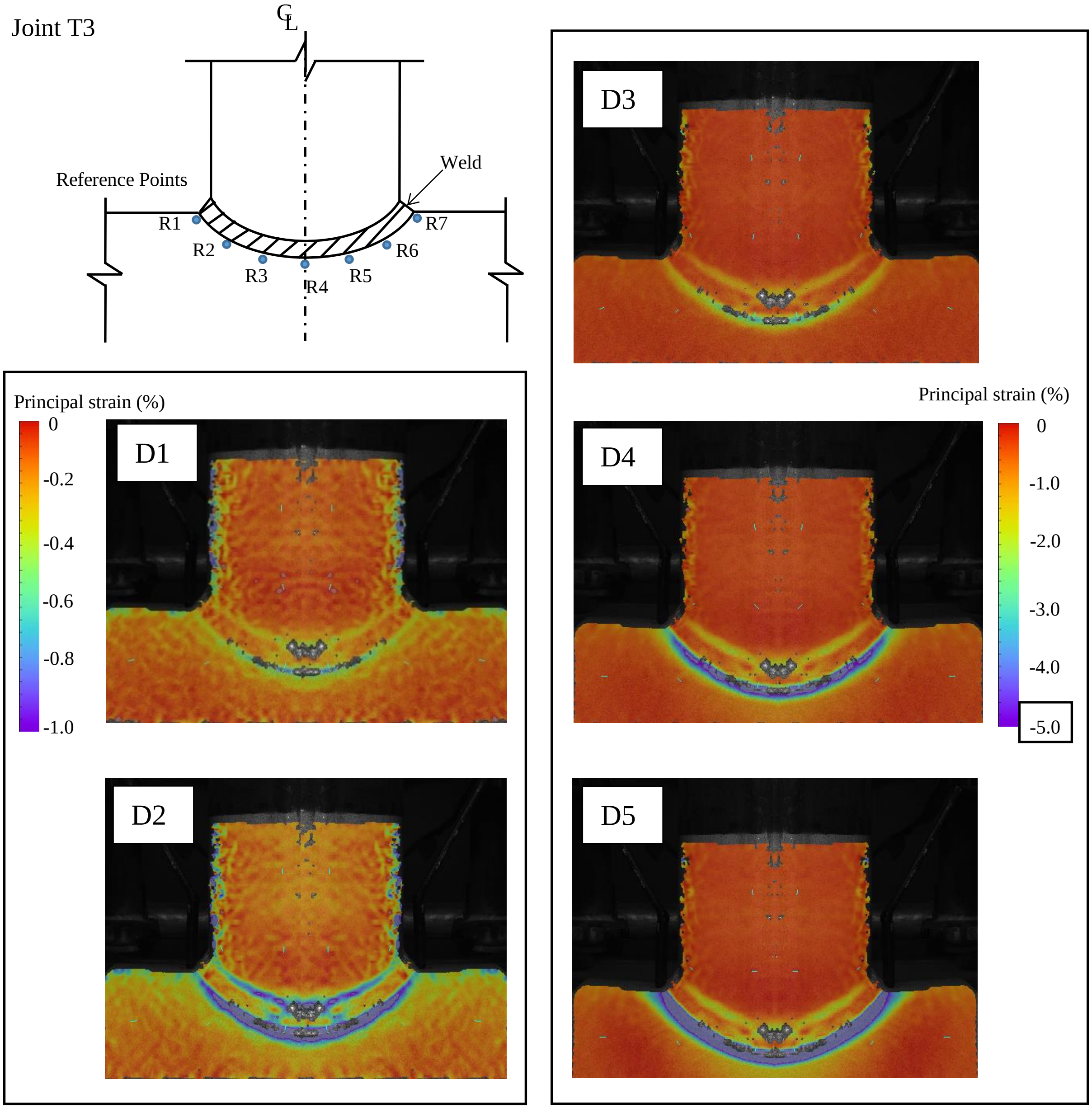

a) Principal strains in various deformation stages

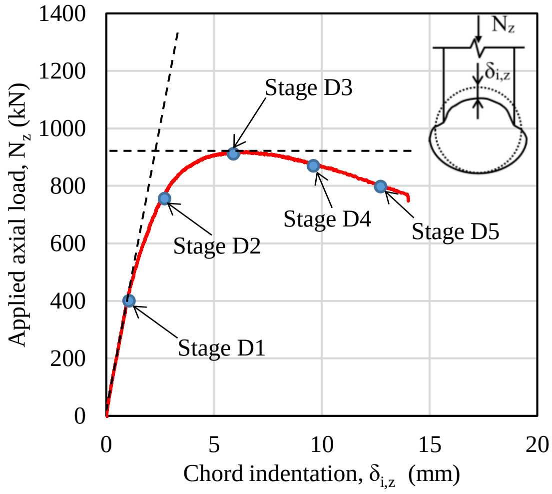

b) Load -indentation curve

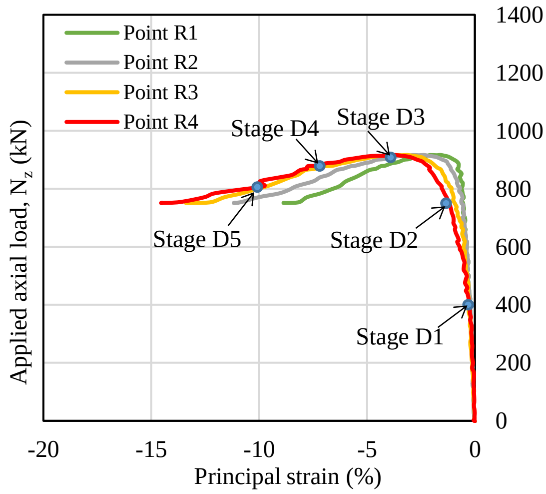

c) Load-principal strain curves

Figure 21 Typical strain contours of the welded brace/chord junction of Joint T3

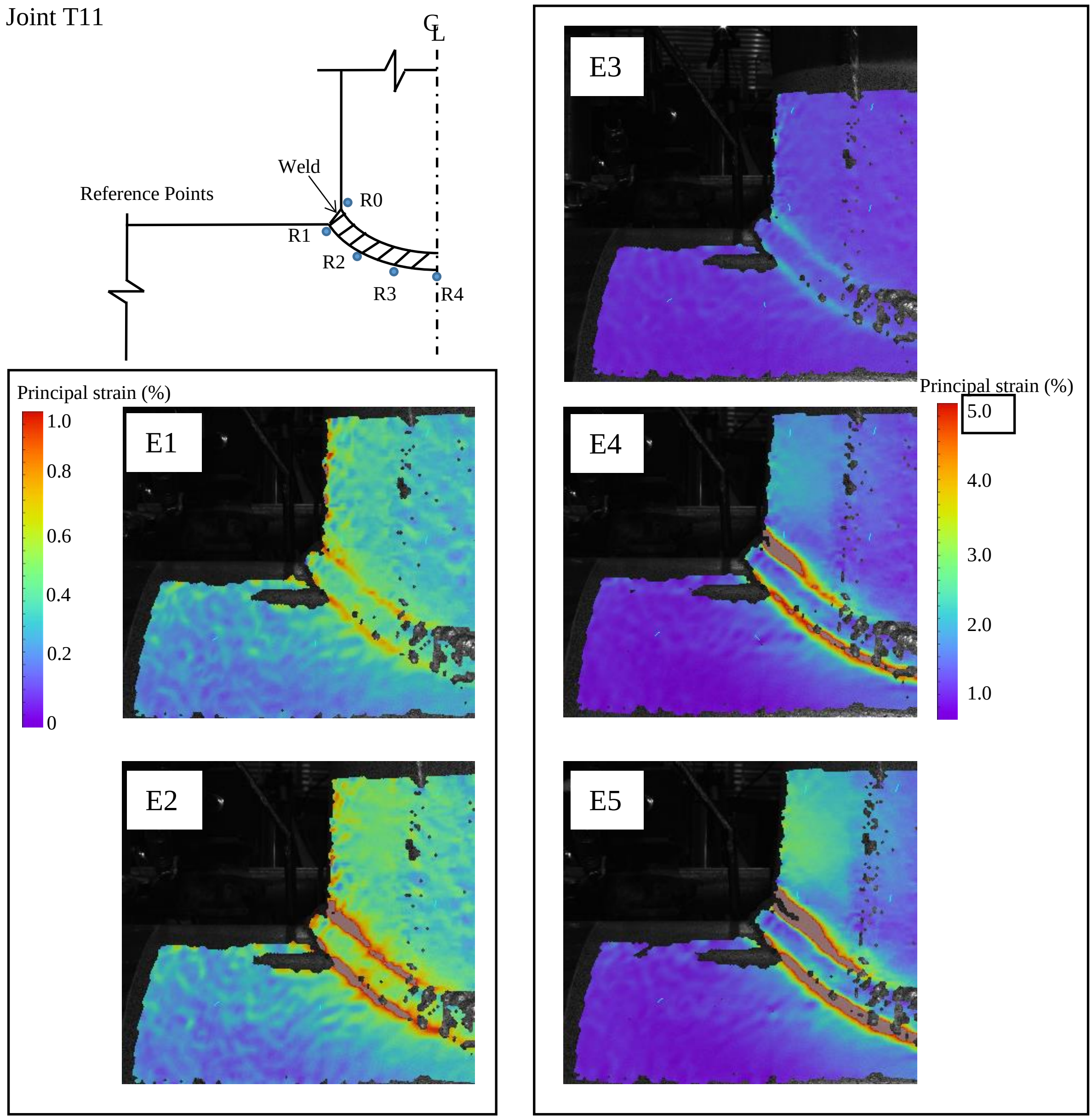

a) Principal strains in various deformation stages

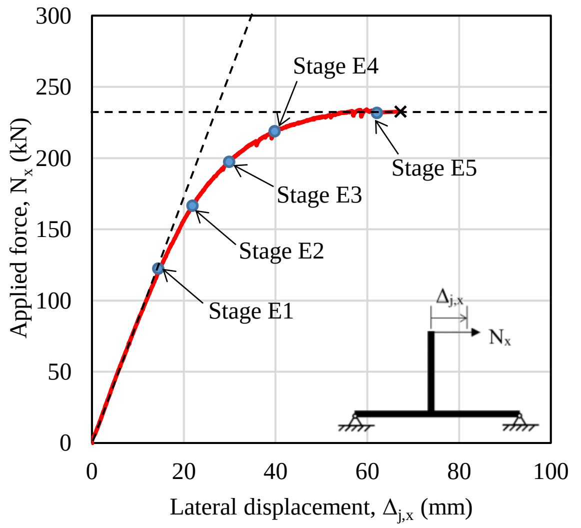

b) Load -indentation curve

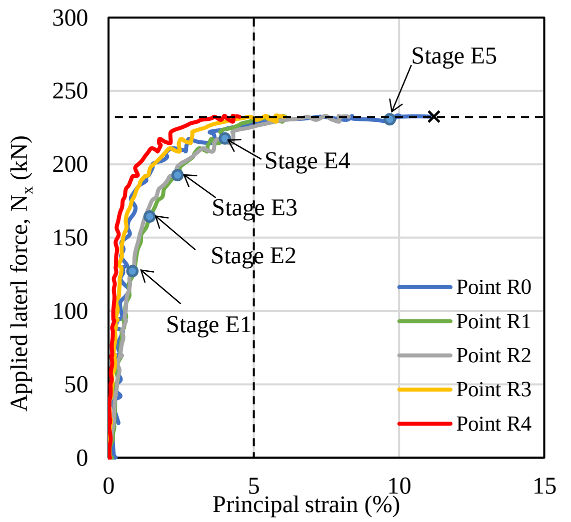

c) Load-principal strain curves

Figure 22 Typical strain contours of the welded brace/chord junction of Joint T11

Table 1 Test programme for T-joints

Joints	Steel grade	Chord $d_0 \times t_0$ (mm×mm)	*Section class of the chord	Brace $d_1 \times t_1$ (mm×mm)	*Section class of the brace	α	β	γ	τ
T1	S355	250×10	Class 1	150× 6	Class 1	9.6	0.6	12.5	0.6
T2	S690	250×10	Class 3	150× 6	Class 3	9.6	0.6	12.5	0.6
T3	S690	250×10	Class 3	150× 6	Class 3	9.6	0.6	12.5	0.6
T4	S355	250×10	Class 1	200× 6	Class 2	9.6	0.8	12.5	0.6
T5	S690	250×10	Class 3	200× 6	Class 4	9.6	0.8	12.5	0.6
T6	S690	250×10	Class 3	200×10	Class 2	9.6	0.8	12.5	1.0
T7	S355	250×10	Class 1	150× 6	Class 1	9.6	0.6	12.5	0.6
T8	S690	250×10	Class 3	150× 6	Class 3	9.6	0.6	12.5	0.6
T9	S690	250×10	Class 3	150× 6	Class 3	9.6	0.6	12.5	0.6
T10	S355	250×10	Class 1	200× 6	Class 2	9.6	0.8	12.5	0.6
T11	S690	250×10	Class 3	200× 6	Class 4	9.6	0.8	12.5	0.6
T12	S690	250×10	Class 3	200×10	Class 2	9.6	0.8	12.5	1.0

* EN 1993-1-1: Cl. 5.5 and Table 5.2.

Table 2 Measured geometric dimensions of T-joints

Joint	Steel grade	Chord			Brace		
		Length, L_0 (mm)	Diameter, d_0 (mm)	Wall thickness, t_0 (mm)	Length, L_1 (mm)	Diameter, d_1 (mm)	Wall thickness, t_1 (mm)
T1	S355	1199.9	251.6	9.9	599.3	152.3	5.9
T2	S690	1198.8	251.6	10.0	599.4	152.6	5.9
T3	S690	1198.8	251.5	9.9	599.4	152.0	6.0
T4	S355	1201.1	251.5	10.0	599.4	200.5	5.9
T5	S690	1199.0	251.8	9.8	599.2	200.9	6.0
T6	S690	1198.5	251.5	9.9	599.4	201.3	10.0
T7	S355	1199.3	251.6	9.9	599.3	151.4	5.9
T8	S690	1197.9	251.8	9.8	599.2	152.6	5.9
T9	S690	1199.3	251.9	9.9	599.3	152.2	6.0
T10	S355	1200.7	251.5	9.9	599.4	201.5	5.9
T11	S690	1199.6	251.9	9.8	599.2	201.5	6.0
T12	S690	1198.6	251.8	9.9	599.2	201.5	9.9

Table 3 Chemical composition (%) of welding electrodes provided by suppliers

Electrode	C	Si	Mn	P	S	Cr	Ni	Mo	Cu
ER110S-G	0.090	0.80	1.70	0.015	0.015	0.3	1.85	0.6	0.1
E71T-1	0.055	0.38	1.35	0.015	0.010	-	-	-	-

Table 4 Mechanical properties of welding electrodes provided by suppliers

Standard	Electrode	Steel grade	Supplier	Weld method	Diameter (mm)	Yield strength (N/mm^2)	Tensile strength (N/mm^2)	Elongation (%)
AWS A5.28	ER110S-G	S690	Bohler	GMAW	1.2	720	880	15
AWS A5.20	E71T-1	S355	Lanyu	GMAW	1.2	490	580	27

Table 5 Measured weld sizes at crown and saddle points

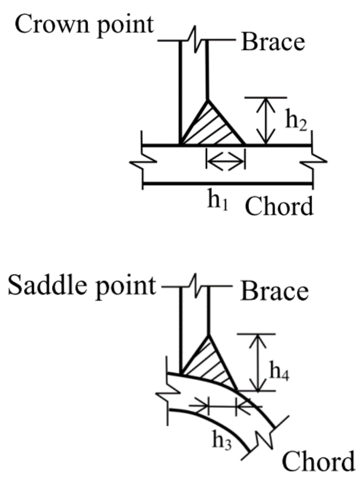

Joint	h_1 (mm)	h_2 (mm)	h_3 (mm)	h_4 (mm)
T1	9.0	11.2	4.3	3.3
T2	10.1	11.5	3.5	3.7
T3	11.0	12.5	3.9	4.0
T4	11.3	12.6	3.3	4.2
T5	11.1	12.9	5.5	4.5
T6	12.0	12.8	1.7	2.7
T7	9.5	11.5	6.9	6.0
T8	9.5	10.8	5.0	4.0
T9	9.9	12.5	4.5	3.5
T10	10.2	11.9	4.0	5.8
T11	12.5	13.0	4.9	4.8
T12	8.9	13.4	2.9	2.5

Table 6 Summary of results of standard tensile tests

	Coupon	Plate thickness (mm)	Young's modulus E (kN/mm^2)	Yield strength f_y (N/mm^2)	Tensile strength f_u (N/mm^2)	f_u / f_y
Curved coupon	S355-BR01	6	208	371	538	1.45
	S355-BR02	6	206	372	533	1.43
	S355-CH04	10	205	365	590	1.62
	S690-BR-01	6	202	747	811	1.08
	S690-BR-02	6	203	745	814	1.09
	S690-BR-03	10	202	749	835	1.12
	S690-CH-04	10	201	766	828	1.08

Note:

For each section, the values of E, f_y and f_u are taken as averaged values of the stress-strain curves shown in Figure 7c).

Table 7 Summary of test results of T-joints between CFCHS under brace axial compression

Joint	Steel grade	Test results		Chord moment resistances			Brace axial resistances					
							CIDECT			EN1993-1-8		
		Failure mode	$N_{z,Rt}$ (kN)	$M_{j,Rt}$ (kNm)	$M_{0,R}$ (kNm)	$\frac{M_{j,Rt}}{M_{0,R}}$	Q_f	$N_{z,R}$ (kN)	$\frac{N_{z,Rt}}{N_{z,R}}$	k_p	$N_{z,R}$ (kN)	$\frac{N_{z,Rt}}{N_{z,R}}$
T1	S355	CP	544	183.6	210.4	0.87	0.74	399	1.36	0.74	352	1.55
T2	S690	CP	861	290.6	441.5	0.66	0.76	780	1.10	0.79	631	1.36
T3	S690	CP	920	310.5	441.5	0.70	0.76	780	1.18	0.79	631	1.46
T4	S355	CP	679	220.7	210.4	**1.05**	0.64	538	1.15	0.64	459	1.48
T5	S690	CP	1223	397.5	441.5	0.90	0.68	1075	1.12	0.70	843	1.45
T6	S690	CP	1175	381.8	441.5	0.86	0.68	1075	1.08	0.70	843	1.39

Notes:

$N_{z,Rt}$ denotes the measured axial resistance of a T-joint.

$N_{z,R}$ denotes the axial resistance predicted to CIDECT or EN 1993-1-8 with a reduction factor for high strength steels.

$M_{j,Rt}$ denotes the measured moment resistance in the chord of a T-joint.

$M_{0,R}$ denotes the basic plastic moment resistance of the chord to EN 1993:1.

Q_f denotes the chord stress function to Design Guide 1 of CIDECT.

k_p denotes the chord stress function to EN 1993-1-8.

CP denotes a local failure mode of chord plastification

Table 8 Summary of test results of T-joints between CFCHS under brace in-plane bending

a) CIDECT

Joint	Steel grade	Test results			Back analysis						Test results
		Failure mode	Resistances		Chord plastification		Chord punching shear		Brace failure		Deformations
			$N_{x,Rt}$ (kN)	$M_{j,Rt}$ (kNm)	$M_{j,R}$ (kNm)	$\frac{M_{j,Rt}}{M_{j,R}}$	$M_{j,R}$ (kNm)	$\frac{M_{j,Rt}}{M_{j,R}}$	$M_{1,R}$ (kNm)	$\frac{M_{j,Rt}}{M_{1,R}}$	Δ_u (mm)
T7	S355	BF	76.4	55.0	49.9	1.10	47.6	1.16	**46.2***	1.19	> 135.0
T8	S690	BF	132.7	99.9	94.3	1.06	**90.0***	1.11	93.0	1.07	84.7
T9	S690	BF	134.2	101.8	94.3	1.08	**90.0***	1.13	93.0	1.09	87.7
T10	S355	BF	138.5	101.1	88.8	1.14	84.7	1.19	**83.8***	1.21	> 104.6
T11	S690	BF	234.2	175.0	167.7	1.04	**159.9***	1.09	168.3	1.04	67.7
T12	S690	CP-S	243.3	178.2	167.7	1.06	**159.9***	1.11	269.2	0.66	88.4

Notes:

BF denotes a brace failure: yielding in a S355 brace, or HAZ fracture in a S690 brace;
CP-S denotes a failure mode of chord punching shear.

$N_{x,Rt}$ denotes the measured lateral resistance of a T-joint.

$M_{j,Rt}$ denotes the measured moment resistance of a T-joint.
$M_{j,R}$ denotes the joint moment resistance predicted to various failure modes.
$M_{1,R}$ denotes the full plastic moment resistance of the brace.
* denotes the smallest value among the design resistances to the three failure modes.

Δ_u denotes the joint displacement at failure

b) EN 1993-1-8

Joint	Steel grade	Test results			Back analysis						
		Failure mode	$N_{x,Rt}$ (kN)	$M_{j,Rt}$ (kNm)	Chord plastification		Chord punching shear		Brace failure		Displacement at failure
					$M_{j,R}$ (kNm)	$\frac{M_{j,Rt}}{M_{j,R}}$	$M_{j,R}$ (kNm)	$\frac{M_{j,Rt}}{M_{j,R}}$	$M_{1,R}$ (kNm)	$\frac{M_{j,Rt}}{M_{1,R}}$	Δ_u (mm)
T7	S355	BF	76.4	58.1	56.3	1.03	47.4	1.23	**46.2***	1.26	> 135.0
T8	S690	BF	132.7	100.9	94.6	1.07	**79.6***	1.27	93.0	1.08	84.7
T9	S690	BF	134.2	102.0	94.6	1.08	**79.6***	1.28	93.0	1.10	87.7
T10	S355	BF	138.5	105.3	100.1	1.05	84.3	1.25	**83.8***	1.26	> 104.6
T11	S690	BF	234.2	178.0	168.1	1.06	**141.5***	1.26	168.3	1.06	67.7
T12	S690	CP-S	243.3	184.9	168.1	1.10	**141.5***	1.31	269.2	0.69	88.4

Notes:

BF denotes a brace failure: yielding in a S355 brace, or HAZ fracture in a S690 brace;

CP-S denotes a failure mode of chord punching shear

* denotes the smallest value among the design resistances to the three failure modes.